

Published in final edited form as:

*Nat Cell Biol.* 2020 July 01; 22(7): 767–778. doi:10.1038/s41556-020-0536-6.

## Heterochromatin establishment during early mammalian development is regulated by pericentromeric RNA and characterized by non-repressive H3K9me3

Adam Burton<sup>1</sup>, Vincent Brochard<sup>2</sup>, Carmen Galan<sup>3,11</sup>, Elias R. Ruiz-Morales<sup>1</sup>, Quirze Rovira<sup>4</sup>, Diego Rodriguez-Terrones<sup>1</sup>, Kai Kruse<sup>4</sup>, Stéphanie Le Gras<sup>5</sup>, Vishnu S. Udayakumar<sup>6</sup>, Hang Gyeong Chin<sup>6</sup>, André Eid<sup>1,12</sup>, Xiaoyu Liu<sup>7</sup>, Chenfei Wang<sup>7</sup>, Shaorong Gao<sup>7</sup>, Sriharsa Pradhan<sup>6</sup>, Juan M. Vaquerizas<sup>4,10</sup>, Nathalie Beaujean<sup>2,8</sup>, Thomas Jenuwein<sup>3</sup>, Maria-Elena Torres-Padilla<sup>1,9,\*</sup>

<sup>1</sup>Institute of Epigenetics and Stem Cells, Helmholtz Zentrum München D-81377 München, Germany

<sup>2</sup>Université Paris-Saclay, INRAE, ENVA, BREED U1198, 78350, Jouy-en-Josas, France

<sup>3</sup>Department of Epigenetics, Max Planck Institute of Immunobiology and Epigenetics, Stübeweg 51, D-79108 Freiburg, Germany

<sup>4</sup>Max Planck Institute for Molecular Biomedicine, 48149 Münster, Germany

<sup>5</sup>Institut de Génétique et de Biologie Moléculaire et Cellulaire, CNRS/INSERM U964, U de S, F-67404 Illkirch, CU de Strasbourg, France

<sup>6</sup>New England Biolabs, Inc., Ipswich, MA 01938

<sup>7</sup>Clinical and Translational Research Center of Shanghai First Maternity & Infant Hospital, School of Life Sciences and Technology, Tongji University, Shanghai, 200092, China

<sup>8</sup>Université Lyon 1, Inserm, Stem Cell and Brain Research Institute U1208, F-69500 Bron, France

<sup>9</sup>Faculty of Biology, Ludwig Maximilians University, Munich, Germany

<sup>10</sup>MRC London Institute of Medical Sciences, Institute of Clinical Sciences, Faculty of Medicine, Imperial College London, Du Cane Road, London W12 0NN, UK

### Abstract

Users may view, print, copy, and download text and data-mine the content in such documents, for the purposes of academic research, subject always to the full Conditions of use: [http://www.nature.com/authors/editorial\\_policies/license.html#terms](http://www.nature.com/authors/editorial_policies/license.html#terms)

\*Corresponding author: torres-padilla@helmholtz-muenchen.de, Tel. + 49(0) 89-3187-3317, Fax. + 49(0) 89-3187-3389.

<sup>11</sup> Present address: *Inmunología y Genética Aplicada SA, Madrid, Spain*

<sup>12</sup> Present address: *The Francis Crick Institute, London NW1 1AT, United Kingdom*

#### Author contributions

A.B. and M.E.T.P. conceived the project and wrote the manuscript. A.A., V.B., C.G., H.G.C. and A.E. performed and designed experiments with the supervision of N.B., T.J., S.P. and M.E.T.P. E.R.R.-M., Q.R., D.R.-T., K.K., S.I.G., V.S.U., X.L., C.W., performed and designed computational analysis with the supervision of S.G., S.P., J.M.V., M.E.T.P.

#### Competing interests

The authors declare no competing financial interest.

Upon fertilization in mammals the gametes are reprogrammed to create a totipotent zygote, a process that involves *de novo* establishment of chromatin domains. A major feature occurring during preimplantation development is the dramatic remodeling of constitutive heterochromatin, although the functional relevance of this is unknown. Here we show that heterochromatin establishment relies on the stepwise expression and regulated activity of Suv39h enzymes. Enforcing precocious acquisition of constitutive heterochromatin results in compromised development and epigenetic reprogramming, demonstrating that heterochromatin remodeling is essential for natural reprogramming at fertilization. We find that *de novo* H3K9 trimethylation in the paternal pronucleus after fertilization is catalyzed by Suv39h2 and that pericentromeric RNAs inhibit Suv39h2 activity and reduce H3K9me3. *De novo* H3K9me3 is initially non-repressive for gene expression but instead can bookmark promoters for compaction. Overall, we uncover the functional importance for the restricted transmission of constitutive heterochromatin during reprogramming and a non-repressive role for H3K9me3.

## Keywords

pre-implantation embryo; epigenetic reprogramming; H3K9me3; RNA

---

## Introduction

The remodeling of histone modifications, particularly of heterochromatin after fertilisation is thought to be required for epigenetic reprogramming and the acquisition of totipotency. However, whether and how constitutive heterochromatin pathways regulate gene expression, chromatin structure and/or reprogramming *in vivo* in the early mammalian embryo remains elusive. Here, we set out to investigate the role of heterochromatin in the mouse embryo immediately after fertilization, specifically to address whether tri-methylation of H3K9 plays a regulatory role at the onset of development.

Mouse embryos start development with a parental epigenetic asymmetry whereby the maternal chromatin is enriched with constitutive heterochromatic histone modifications, while the paternal genome is largely devoid of them<sup>1-3</sup>. Global levels of histone modifications associated with constitutive heterochromatin, such as H3K9me3, H3K64me3 and H4K20me3 decrease sharply after fertilization<sup>4-7</sup>. The Suv39h1 and Suv39h2 histone methyltransferases are key players in the catalysis of H3K9me3 at constitutive heterochromatin regions on the genome<sup>8-10</sup>. However, how heterochromatin is first established in mammals remains unknown.

## Results

### De novo H3K9me3 activity occurs immediately after fertilization

The global decrease of H3K9me3 levels after fertilization has been correlated with low levels of *Suv39h1* mRNA<sup>4,11</sup> (Fig. 1a), which is reflected in the absence of detectable Suv39h1 protein until the 8-cell stage (Fig. 1b and Extended Data Fig. 1a). However, when carefully examining H3K9me3 levels, we observed that while early zygotes immediately after fertilization displayed no detectable H3K9me3 in the paternal pronucleus, late zygotes

showed a clear accumulation of H3K9me3 (Fig.1c). This is in agreement with recent H3K9me3 ChIP-seq data in mouse preimplantation embryos showing acquisition of H3K9me3 in the paternal genome in zygotes<sup>12</sup>. Although a minor proportion of these regions are also detectable in sperm, potentially suggesting a low level inheritance undetectable by immunofluorescence, these results were intriguing and indicate a previously unappreciated *de novo* H3K9 methylation activity in the first cell cycle after fertilization.

To determine which HMT catalyses *de novo* H3K9 methylation, we first examined the expression of the second *Suv39h* gene, *Suv39h2*, which indicated that *Suv39h2* transcripts are abundant in oocytes and early embryos<sup>4,13,14</sup> (Fig.1d). *Suv39h2* protein showed a greater enrichment in the paternal pronucleus than the maternal pronucleus in late zygotes (Fig.1e and Extended Data Fig.1b-c), in contrast to *Suv39h1*, which was undetectable in both pronuclei (Fig.1b). However, we did not detect *Suv39h2* in early zygotes (Extended Data Fig.1d). Instead, *Suv39h2* accumulation in the paternal pronucleus correlated with H3K9me3 appearance, and persisted through the 8-cell stage (Fig.1c and 1e). To address whether *Suv39h2* is responsible for *de novo* H3K9me3, we performed RNAi against *Suv39h2* in early zygotes (Fig.1f and Extended Data Fig.1e). RNAi for *Suv39h2* led to a strong depletion of H3K9me3 in the paternal pronucleus, in contrast to the controls (Fig.1g-h). H3K9me3 levels continued to decrease in the 2-cell stage upon *Suv39h2* RNAi (Extended Data Fig.1f-g), suggesting that changes in H3K9me3 are more dynamic than previously anticipated, in agreement with recent data<sup>12</sup>. We did not observe change in H3K9me3 levels on the maternal chromatin after *Suv39h2* RNAi, suggesting either a localised reduction of H3K9me3 undetectable by this method or that a different methyltransferase may be responsible for the reported H3K9me3 acquisition here<sup>12</sup>. Thus, *de novo* H3K9me3 on the paternal chromatin is catalysed by *Suv39h2*. Moreover, *Suv39h1* and *Suv39h2* proteins display contrasting patterns of expression in early embryogenesis.

### Pericentromeric RNA modulates *Suv39h2* activity and reduces H3K9me3 levels in zygotes

The contrasting expression patterns of *Suv39h1* and *Suv39h2* prompted us to investigate potential biochemical differences between the two KMTs. The mouse *Suv39h2* – but not *Suv39h1* – harbours an extended N-terminal domain<sup>14</sup> (Fig.2a) that can bind RNA *in vitro*<sup>15</sup>. This basic domain provides an additional RNA affinity to *Suv39h2*, although both full-length *Suv39h1* and full-length *Suv39h2* can broadly interact with single and double-stranded nucleic acids<sup>16,17</sup>. This, along with previous studies showing that pericentric H3K9me3 foci are dispersed upon RNaseA treatment<sup>18</sup>, prompted us to investigate whether H3K9me3 is regulated by RNA in embryos. Because major satellite (MajSat) transcripts from the pericentromere are transcribed primarily from the paternal genome from both strands in zygotes<sup>4,19,20</sup>(Fig.2b), we considered them as potential candidates regulating *Suv39h2* activity. We generated full-length recombinant *Suv39h1* and *Suv39h2* and incubated each of them with increasing MajSat dsRNA concentrations to allow for RNA binding, after which we performed KMT assays using histone H3.1 (Fig.2c). *Suv39h2* activity was attenuated with increasing concentrations of dsRNA, whereas we did not observe a reduction of *Suv39h1* activity across the dsRNA concentrations tested (Fig.2c). Thus, we conclude that *Suv39h2* KMT activity can be modulated by MajSat dsRNA. To address whether RNA modulation of *Suv39h2* activity also occurs *in vivo*, we microinjected

*in vitro* transcribed pericentromeric dsRNA into the paternal pronucleus of mid-stage zygotes<sup>20</sup>, and interrogated global levels of H3K9me3 in late zygotes (Fig.2d). Remarkably, H3K9me3 was undetectable in the paternal pronuclei of zygotes in which we injected pericentromeric dsRNA, but not ssRNA (Fig.2e-f and Extended Data Fig.2a-b). To further assess whether endogenous MajSat transcripts can regulate H3K9me3, we targeted VP64 to MajSat using TALE<sup>21</sup> in zygotes to activate the endogenous locus. Consistent with the above, this resulted in a reduction of H3K9me3 throughout the paternal pronucleus (Fig.2g-h). Thus, pericentromeric RNA has a regulatory function and can inhibit endogenous Suv39h2 activity, thereby attenuating H3K9me3 levels in the early mouse embryo.

### H3K9me3 is non-repressive during early preimplantation development

Next we addressed the biological significance of *de novo* H3K9me3 catalysed by Suv39h2. For this, we first analysed H3K9me3 ChIP-seq data from zygotes from C57/B16 X DBA crosses<sup>12</sup>. We sorted genes based on their enrichment of H3K9me3 on either the paternal (DBA) or maternal (C57/B16) chromatin. This analysis revealed a few genes with strong H3K9me3 enrichment on the paternal allele (Fig.3a-b), indicating *de novo* H3K9me3 accumulation on these regions, in agreement with our immunostaining results and with previous ChIP-seq analysis<sup>12</sup>. As expected, H3K9me3 was also present across the maternal genome (Fig.3a-b). Likewise, H3K9me3 was enriched at some repeat families on the paternal chromatin, particularly across LTRs in agreement with previous analysis (Extended Data Fig.3a and Table S1)<sup>12</sup>. SINE elements were generally found in regions enriched with paternal H3K9me3 (Extended Data Fig.3a). Other TE types such as LTRs from the ERV-K (IAPs) and RLTR families were clearly decorated with H3K9me3 peaks (Extended Data Fig.3b). In contrast, most LINE-1 elements were found in regions depleted of paternal H3K9me3 (Extended Data Fig.3a). We conclude that H3K9me3 is distributed on specific regions of the paternal genome.

Secondly, we asked whether *de novo* H3K9me3 regulates gene expression. For this, we first performed RNA-seq in late 2-cell stage embryos after Suv39h2 RNAi (Table S2). Surprisingly, we found that only 141 genes differentially expressed ( $P_{adj} < 0.05$ ), among which more genes (60%;  $n=83$ ) were down-regulated upon Suv39h2 knockdown (Fig.3c and Table S3). In addition, only 5 transposable elements displayed significant changes in expression (Fig.3d and Table S3). We confirmed these results using RT-QPCR for selected genes and repeats (Extended Data Fig.3c-d and Table S4). Thus, *de novo* H3K9me3 catalysed by Suv39h2 is unlikely to regulate gene expression globally, including the expression of transposable elements. In line with our conclusions on a non-repressive role of *de novo* H3K9me3, we did not observe a major developmental defect upon RNAi for Suv39h2, since zygotes injected with dsRNA for Suv39h2 formed blastocysts at a similar rate to control RNAi, and displayed no obvious morphological defects (Extended Data Fig.3e).

Next, we addressed whether the few genes up and down-regulated upon Suv39h2 knockdown are enriched in H3K9me3. Remarkably, the majority of down-regulated genes upon Suv39h2 RNAi are enriched in H3K9me3 at the TSS in 2-cell stage embryos, acquiring signal from the mid zygote to the late 2-cell stage (Fig.3e). In contrast,

upregulated genes showed little or no enrichment of H3K9me3. Thus, depletion of Suv39h2 results in downregulation of some H3K9me3-enriched genes, suggesting that early deposition of H3K9me3 is compatible with gene expression. To address this hypothesis, we extracted the top 500 genes showing highest paternal and maternal H3K9me3 enrichment and investigated their expression throughout development using published RNA-seq datasets<sup>22</sup>. Transcripts of paternal-H3K9me3-enriched genes were more abundant than the maternal-enriched H3K9me3 counterpart (Fig.3f). Many of these genes were robustly expressed, reinforcing the hypothesis that H3K9me3 is compatible with gene expression at these stages (Fig.3g). However, differences in expression resolved gradually over cleavage stages (Fig.3f), implying that early marking of H3K9me3 may predispose for repression at later developmental times. To address this possibility, we first asked if H3K9me3 enrichment correlates with chromatin accessibility. Surprisingly, analysis of ATAC-seq data from early embryos<sup>23</sup> revealed that genes paternally enriched with H3K9me3 display an average open chromatin configuration in early cleavage stages (Fig.3h). Secondly, we assayed chromatin accessibility in embryos upon Suv39h2 depletion using NicE-seq (Extended Data Fig.3f), which revealed that Suv39h2 loss in zygotes results in an increased proportion of accessible promoters at the 8-cell stage (Fig.3i). These data suggest that *de novo* H3K9me3 on the paternal chromatin primes genomic regions for chromatin compaction at later developmental stages. Importantly, our data indicate a non-repressive function of H3K9me3 at the beginning of development.

### Induction of constitutive heterochromatin compromises development

The above data together indicate that the earliest developmental stages are characterized by a Suv39h2-driven H3K9me3 pathway whose activity is regulated by pericentromeric RNA and is largely non-repressive for gene expression. To address whether the absence of mature constitutive heterochromatin is due to the absence of SUV39H1 in early cleavage stages, we undertook a gain-of-function approach in zygotes (Fig.4a). Microinjection of HA-*Suv39h1wt* mRNA led to a robust expression of SUV39H1 in both pronuclei (Fig.4b), which persisted until the 4-cell stage, but not later (Fig.4c and Extended Data Fig.4a). Because ChIP approaches are not currently feasible in microinjected embryos, we addressed whether Suv39h1wt expression leads to global changes in chromatin using quantitative immunofluorescence. Expression of Suv39h1wt led to a robust increase in global H3K9me3 levels at the 2-cell stage compared to controls ( $2.7 \pm 0.15$  fold) (Fig.4d, Extended Data Fig.4b and Supplementary Videos 1–2), which appeared distributed throughout the nucleus, with an obvious enrichment in DAPI-rich regions. These DAPI-rich regions corresponded to regions of MajSat, as determined by labelling major satellites using a dCas9-mClover fusion protein (Fig.4e), suggesting changes in nuclear organization of pericentromeric chromatin. Indeed, an analysis of CENP-A and MajSat localization revealed a striking rearrangement of chromocentres at the 2-cell stage, which appeared in stronger, fewer and more clustered foci in embryos expressing Suv39h1wt, compared to controls (Fig.4e-f). Thus, Suv39h1wt gain-of-function results in precocious chromocenter formation. The increase in global H3K9me3 in 2-cell stage embryos was specific to Suv39h1, since expression of equimolar concentrations of mRNA for other H3K9-specific methyltransferases Setdb1, Setdb2 or Ehmt2/G9a did not lead changes in global H3K9me3 levels to the extent of Suv39h1wt (Extended Data Fig.4c-d). Suv39h1 activity also resulted in the accumulation of H4K20me3

in the pericentromeric chromatin<sup>24</sup> in a large proportion of embryos (Fig.4g). In contrast, H4K20me3 was not detectable in the majority of control 2-cell stage embryos (Fig.4g), as previously reported<sup>7, 25</sup>. Suv39h1wt expression led to a robust accumulation of H3K64me3, throughout the nuclei of 2-cell stage embryos, contrary to the controls where H3K64me3 is absent<sup>6</sup> (Fig.4h and Extended Data Fig.4e). We observed no increase in global levels of H3K9me3, H4K20me3 or H3K64me3 upon expression of the catalytic dead enzyme (Suv39h1mut; Fig.4d,g-h, Extended Data Fig.4b and e, Supplementary Video 3). We conclude that expression of Suv39h1wt in zygotes leads to the premature establishment of constitutive heterochromatin and chromocenter formation, suggesting that the absence of Suv39h1 is the limiting factor controlling constitutive heterochromatin establishment after fertilization.

To address whether the delayed acquisition of constitutive heterochromatin is relevant for development, we tested the effect of Suv39h1wt expression on developmental progression (Fig.5a). Importantly, Suv39h1wt expression led to a strong developmental arrest, with only 27 % of embryos reaching the blastocyst stage, even after extended culture (Fig.5b). In contrast, control non-injected embryos and embryos expressing GFP alone formed blastocysts at significantly higher rates, of 93 % and 75 %, respectively (Fig.5b). Embryos expressing Suv39h1mut developed at similar rates to the control injections demonstrating that the phenotype depends on Suv39h1 methyltransferase activity (Fig.5b). The specific developmental arrest elicited by Suv39h1wt in comparison to Suv39h1mut appeared at the morula stage, without an obvious morphological effect on compaction (Extended Data Fig.4h). These embryos showed misregulation of genes involved in pluripotency (*Myc*, *Klf4*) and lineage allocation (*Pdgfra*, *Pou5f1/Oct4*, *Tead4*, *Gata6*, *Fgfr2*, *Cdx2*) (Extended Data Fig.5a and Tables S5–6). Accordingly, quantitative immunostaining and 3D-reconstruction of the Suv39h1wt-injected embryos that reached the blastocyst stage revealed a failure to segregate cells into the two blastocyst lineages and to fully repress NANOG in the trophectoderm (Extended Data Fig.5b-d). This effect was specific to Suv39h1. Indeed, expression of Suv39h2 in zygotes using the same experimental design as for Suv39h1 (Fig.5c) resulted in a similar increase in global H3K9me3 levels at the 2-cell stage compared to Suv39h1 (Fig.5d-e). However, Suv39h2 expression did not affect developmental progression and embryos formed blastocysts in the same proportion as controls (Fig.5f). In addition, ectopic expression of a different heterochromatic methyltransferase, Suv420h1, had no effect on embryo development<sup>26</sup>. Our results indicate that the acquisition of a global chromatin configuration with typical constitutive heterochromatic features, namely H3K9me3, H4K20me3, H3K64me3 and chromocentres, is not compatible with early developmental progression.

To investigate a potential effect of Suv39h1-mediated H3K9me3 on gene expression, we performed RNA-seq in late 2-cell stage embryos, the timepoint at which zygotic genome activation occurs<sup>27</sup>. Unexpectedly, our transcriptional profiling revealed only minor changes in gene expression between Suv39h1wt and control Suv39h1mut-injected groups (39 upregulated and 19 downregulated genes) (Fig.6a and Table S7). Similarly, most repeat families were unaffected (Fig. 6b and Table S8). We validated our RNA-seq using high throughput RT-qPCR in single embryos, which confirmed no significant changes in the expression of the genes or repetitive elements assayed (Extended Data Fig. 6a and Table S4).

These experiments rule out a global down-regulation of transcription in embryos expressing Suv39h1. We conclude that expression of Suv39h1 and the resulting increase in H3K9me3 do not drastically affect gene expression or zygotic genome activation at the 2-cell stage.

To address when gene expression changes arise and assess potential phenotypic heterogeneity, we performed single embryo RNA-seq at consecutive timepoints from the 2-cell stage through to the morula stage, combined with pseudotime analysis (Table S9). This revealed a defect in the gene expression programme at the 4-cell stage in the majority of embryos expressing Suv39h1 wt (Fig. 6c-d and Table S10). We found 200 misregulated genes at this stage, the majority of which were upregulated (71%), supporting a non-repressive function for H3K9me3. Interestingly, we found that the majority of upregulated genes are normally 2-cell stage-specific genes (Fig. 6e). Thus, Suv39h1 gain-of-function leads to a failure to downregulate a portion of the 2-cell stage gene expression program. In addition we found that genes like *Cdx2* - a regulator of the trophectoderm - and *Dppa1* - developmental pluripotency associated-1, were downregulated at the morula stage (Table S10). Overall, our data suggests that the phenotype elicited upon Suv39h1 expression emerges heterogeneously at the 4-cell stage partly due to a defective downregulation of a significant fraction of the 2-cell stage gene expression program but also through precocious formation of chromocentres, and culminates with the failure to achieve a complete resolution of cell fate upon blastocyst formation.

### Suv39h1 expression inhibits epigenetic reprogramming

The above results suggest that enforcing Suv39h1-driven H3K9me3 and the consequent constitutive heterochromatic features after fertilization prevents epigenetic reprogramming *in vivo*. However, the experimental setup above does not distinguish between effects on development versus those on epigenetic reprogramming since they both occur in parallel during cleavage stages<sup>28</sup>. To address directly whether Suv39h1 wt expression affects epigenetic reprogramming *in vivo*, we performed nuclear transfer (NT) in enucleated oocytes, using ES cell nuclei as donor (Fig.7a). We microinjected *Suv39h1 wt* mRNA after NT to enforce de novo H3K9me3 during reprogramming. Although it has been demonstrated that depleting donor somatic nuclei of H3K9me before NT improves cloning efficiency<sup>29</sup>, the role of *de novo* H3K9me3 at the onset of reprogramming, after nuclear transfer, is unknown. We used two negative controls for potential micromanipulation effects; GFP and for H2B-Cherry. Expression of Suv39h1 wt after NT resulted in a strong increase of H3K9me3 in 2-cell stage cloned embryos compared to the negative controls, which showed instead the typical dispersed H3K9me3 pattern upon NT<sup>30,31</sup> (H2B-cherry, Fig.7b). Scoring the number of cloned embryos that developed past the 2-cell stage, an indicator of successful reprogramming<sup>30,32</sup>, revealed a significantly lower rate of reprogramming with Suv39h1 wt ( $P=0.014$  and  $P=0.006$ , for the two experimental conditions, respectively)(Fig.7c). We also analysed the number of nucleolar-like bodies (NLBs), which reflects changes in nuclear organisation indicative of successful reprogramming<sup>33</sup>. Suv39h1 wt led to a significant reduction in the number of NLBs ( $4.4 \pm 0.4$  vs  $6.7 \pm 0.4$   $P=1.1 \times 10^5$ )(Extended Data Fig. 6b). The decrease in the developmental capacity of cloned embryos at the 2-cell stage indicates a defect in reprogramming, which was exacerbated progressively, since none of the embryos expressing Suv39h1 after NT formed blastocysts (Fig.7d and Extended Data Fig.

6c). The effect on NT efficiency was dependent on the methyltransferase activity of Suv39h1 (Extended Data Fig. 6e). Thus, Suv39h1 blocks epigenetic reprogramming upon NT. The above results together show that Suv39h1-mediated H3K9me3 in early embryogenesis is detrimental for developmental progression and epigenetic reprogramming.

## Discussion

Our results suggest that both a stepwise expression profile and regulation of the methyltransferase activity of Suv39h enzymes ensures low levels of H3K9me3 after fertilization (Fig. 7e). In addition, Suv39h1 and Suv39h2 may potentially target different genomic regions, which, together with their distinct temporal expression patterns, may contribute to the regulation of heterochromatin establishment in the embryo. Assessing direct targets of Suv39h1 and Suv39h2 will shed light into a refined mechanism of action of the two Suv39 enzymes. We propose that an ‘early’ immature heterochromatin characterized by low levels of constitutive heterochromatic histone modifications, lack of chromocentres and a globally relaxed chromatin organization is enabled through RNA-regulated Suv39h2. This immature heterochromatin is a hallmark of early mammalian development and is compatible with transcriptional activity. The restriction of ‘late’ mature heterochromatin, characterized by heterochromatic histone modifications, chromocentres, transcriptional repression and a more compact chromatin architecture is controlled by the regulated expression of Suv39h1 and is essential for epigenetic reprogramming at fertilization.

We propose that *de novo* H3K9me3 after fertilization facilitates subsequent establishment of ‘mature’ constitutive heterochromatin at around the time of implantation when other histone modifications of constitutive heterochromatin and DNA methylation start to accumulate<sup>2,34,35</sup>. This is in line with the self-regulatory loop that directs and reinforces Suv39h1-dependent H3K9me3 methylation<sup>36</sup>. Once heterochromatin is established, H3K9me3 plays an important role in lineage establishment and maintenance<sup>37</sup>. The potential impact of Suv39h1/h2 function and the resulting H3K9me3 in regulating DNA methylation dynamics during preimplantation development will be important to address in the future.

H3K9 modifiers can inhibit, but also enhance iPS derivation<sup>38</sup>. During iPS generation, Suv39h1, but not Suv39h2 limits reprogramming efficiency to pluripotency<sup>39,40</sup>. Our data show that enforcing H3K9me3 via Suv39h1 during both natural reprogramming at fertilization and reprogramming to totipotency through NT is also detrimental for reprogramming, while Suv39h2-enabled immature heterochromatin is permissive. Additionally, it would seem that both the H3K9me3 status in the donor nuclei<sup>29,41</sup>, as well as the *de novo* acquisition of H3K9me3 during the first steps of reprogramming once the process has been initiated (this work) are key determinants in reprogramming efficiency. Indeed, ectopic expression of the H3K9 demethylase *Kdm4b* in cloned embryos results in improved NT efficiency<sup>42</sup>. This together, anticipates a dynamic mechanism where a turnover of H3K9me3 levels occurs at different steps of the process.

Our work further indicates that Suv39h1/h2-mediated H3K9me3 does not regulate the transposon repertoire in early development, which contrasts to ES cells<sup>8</sup>. This is in line with recent work indicating that loss of Setdb1, while depleting H3K9me3 from a number LTRs,

for the most part does not affect their transcription at the morula stage<sup>12,43</sup>. In addition loss of Ehmt2/G9a does not lead to significant changes in TE expression<sup>44</sup>. The reported lack of HP1 $\alpha$  expression during preimplantation development<sup>7</sup>, along with other downstream heterochromatic features, such as histone deacetylase activity, may explain the observed non-repressive function of H3K9me3. Nucleosome occupancy<sup>12</sup> may also be a more relevant mediator of transcriptional silencing in the early embryo. Recent work also indicates a non-canonical and transcriptional-neutral accumulation of H3K4me3 in oocytes<sup>45,46</sup>, implying that a non-instructive role for histone modifications in transcriptional regulation may be a widespread feature of early development.

Our work underscores an important role for the dynamic regulation of H3K9me3 levels in the early mouse embryo, identifying a non-repressive function for H3K9me3, and documents a previously unappreciated regulatory role for RNA in restricting heterochromatic H3K9me3 at fertilization.

## Methods

Unless otherwise stated all reagents were purchased from Sigma-Aldrich.

### Embryo collection, microinjection and culture

All mouse experiments were approved by the Ethics Committee of the Université de Strasbourg (Com'eth Institute of Genetics, Molecular and Cellular Biology) and performed under the compliance of French legislation or of the Government of Upper Bavaria. For immunostaining, CD-1 female mice (4-8 weeks old) were mated with CD-1 male mice (3-6 months old) and early and late zygotes, 2-cell and 8-cell stages were collected at 10h, 17h, 38h and 58h post-coitum respectively. For microinjection, embryos were collected from 5-7 week old F<sub>1</sub> (C57BL/6J  $\times$  CBA/H) superovulated females crossed with F<sub>1</sub> males (3-6 months old). Superovulation was induced by intraperitoneal injection of pregnant mare serum gonadotropin (PMSG, Intervet, 5 IU) and human chorionic gonadotropin (hCG, Intervet, 7.5 IU) 46-48 hours later. Embryos were collected at the timepoints after hCG injection indicated in the figure legends. mRNAs were transcribed in vitro from the pRN3P plasmid using the mMACHINE kit (Ambion). All cDNAs were subcloned to include identical 5' cap and untranslated region (UTR) (including Kozak) and 3' UTR to ensure equivalent expression levels. Suv39h1 cDNA was obtained through a generous gift from A. J. Bannister (Gurdon Institute, Cambridge, UK). Suv39h1mut was prepared by site-directed mutagenesis of Suv39h1 at Histidine 324 to Lysine and Cysteine 326 to Alanine<sup>36</sup>. Zygotes were microinjected with 1-2 pl of the indicated mRNAs (600 ng/ $\mu$ l for Suv39h1/Suv39h1mut/Suv39h2 or 250 ng/ $\mu$ l for Gfp) and allocated to the experimental groups at random. Equimolar concentrations of Setdb1 (1.5  $\mu$ g/ $\mu$ l), Setdb2 (900 ng/ $\mu$ l) or G9a/Ehmt2 (1.5  $\mu$ g/ $\mu$ l) mRNA were microinjected. Embryos were cultured in KSOM (K-modified simplex optimized medium) microdrops under oil at 37°C, 5% CO<sub>2</sub>. The dCas9- mClover plasmid was kindly provided by T. Nakatani and we microinjected 50-100ng/ $\mu$ l of mRNA and 20 ng/ $\mu$ l of Major Satellites sgRNA<sup>47</sup>. The TALE-MajSat control and -VP64 mRNAs were microinjected at 600ng/ $\mu$ l.

## In vitro dsRNA preparation

Double-stranded major satellite RNA was prepared as previously described<sup>20</sup> by in vitro transcription from pGEM plasmid (Clontech A1360) containing a 234 bp major satellite repeat unit using MAXIscript SP6/T7 kit (Ambion), followed by hybridisation of the two complementary single-stranded RNAs and treatment with RNaseA and T1 to remove unhybridised single-stranded RNA. 1-2  $\mu$ l of 700 ng/ $\mu$ l major satellite dsRNA and 0.02% dextran-rhodamine was injected into the paternal pronucleus of zygotes. Single-stranded major satellites injection was performed with 1.4  $\mu$ g/ $\mu$ l of the non-hybridised in vitro-transcribed single-stranded RNAs. Double-stranded RNA targeting Suv39h2 was prepared by subcloning the N-terminal region of *Mus musculus* suv39h2 cDNA comprising base pairs 1-380 into the vector pGEM followed by in vitro transcription using the SP6 and T7 polymerases and then hybridization as described above. As a control, 500  $\mu$ g- $\mu$ l of a 460bp region targeting the lacZ comprising base pairs 1568 – 1957 was used. 500  $\mu$ g/ $\mu$ l of purified dsRNA was microinjected into zygotes with 0.02% dextran-rhodamine at the indicated times post-hCG. For in vitro HMT assays, ssRNA was generated by in vitro transcription using the T7 promoter in the EcoRI-linearized pSAT plasmids<sup>48</sup> containing either a single repeat of major satellite cloned in the sense (pSAT-S) or antisense (pSAT-AS) orientation. To generate dsRNA, equimolar amounts of sense and antisense ssRNA were mixed in 1xSSC buffer (150 mM NaCl, 15 mM sodium citrate), incubated 2 min at 90°C in a thermomixer. The temperature was allowed to drop to 60°C and incubated for 5 min, then decreased to 20°C and incubated for 30 min.

## Immunostaining and Confocal Microscopy

Fixation of embryos was performed as described<sup>49</sup>. Briefly, the zona pellucida was removed with Acid Tyrode solution, followed by two washes in PBS and fixation in 4% paraformaldehyde, 0.04% triton, 0.3% tween-20, 0.2% sucrose at 37°C. Embryos were then washed with PBS and permeabilized with 0.05% Triton-X100 for 20 minutes. After permeabilization, embryos were washed 3x in PBSt (0.1% Tween20 in PBS), quenched in 2.6 mg/ml freshly prepared ammonium chloride, washed 3x in PBSt and blocked for 3-4 hours at 4°C in blocking solution (BS: 3% BSA in PBSt) and incubated with primary antibodies in BS. Antibodies used were as follows: anti-Suv39h1 (Cell Signalling 8729), anti-Suv39h2 (Abcam 104343) (1:100), anti-HA (Roche 11867423001), anti-H3K9me3 (Millipore 07-442), anti-H3K9me3 (Active Motif 39286) (1:100) (used only in relation to Fig. 1), anti-H4K20me3 (Millipore 07-463), anti-H3K64me3 (generous gift from S. Daujat IGBMC, France), anti-GFP (Abcam ab13970) (1:1000), anti-CenpA/B (Europa Bioproducts FZ90C-CS1058) (1:500), anti-Cdx2 (BioGenex AM392-5M) (1:500), anti-Nanog (CosmoBio RCAB0002P-F) (1:500), and anti-Oct4 (BD Bioscience 611203). Dilutions were 1:250 unless otherwise indicated. After overnight incubation at 4°C embryos were washed 3x in PBSt, blocked and incubated for 3h at RT in BS containing secondary antibodies labelled with Alexa or Cy3 fluorophores (Invitrogen) (catalog numbers; A32731, A32732, A32733, A10522, A-11029, A-21424, A32728, A-21445, 1:500 dilution). After washing embryos were mounted in Vectashield (Vector Laboratories) containing 4'-6-Diamidino-2-phenylindole (DAPI). Confocal microscopy was performed on a 63x oil objective in a TCS SP8 inverted confocal microscope (Leica). Z-sections were taken every 0.5-1  $\mu$ m. Image analysis was performed using LAS-AF (Leica) and Imaris (Bitplane). Acquisition

parameters were set in order to obtain fluorescence intensity signal in the linear range of hybrid detectors throughout the manuscript. These detectors have negligible detector noise and linearly amplify incoming photons into photoelectrons, allowing the counting of measured photons as long as the detector is not saturated. Hence, given identical acquisition settings, the fluorescence signal recovered accurately reflects the level of antigen present in the system

### Quantification of Fluorescence Intensity

Confocal z-series stacks were reconstructed in 3D using Imaris software (Bitplane) and the pronuclei (zygote) or nuclei (2-cell stage) were segmented based on the DAPI channel. We used 3D images because analysis of optical sections at 0.5 microns apart robustly reflects the intensity distribution throughout the nucleus (see for example refs. 26, 50) more accurately than measuring a single confocal section alone. The average fluorescence intensity for the channel of interest within the segmented region was calculated after background subtraction, based on the cytoplasmic signal. Because the use of a no-primary antibody control reliably resulted in background signal intensity comparable to the cytoplasmic signal intensity we chose to use cytoplasmic signal as the threshold for background subtraction for nuclear antigens targeted in this study, as this should largely originate from secondary antibody non-specific binding. The background threshold was calculated based on the mean cytoplasmic intensity plus two standard deviations of the cytoplasmic signal, thus corresponding to the empirical 95% rule and hence encompassing the majority of unspecific intensity values. The fluorescence intensity for each embryo was normalised to the mean of the non-injected control group, per experiment.

### Nuclear Transfer and Microinjection

Nuclear transfer experiments were performed under the authorization from the departmental veterinary regulatory service (license N° 78–95) and from the local ethics committee (N° 12/123 - Comethea Jouy-en-Josas/AgroParisTech) at INRA. Oocytes were prepared by superovulating eight-week old F1 (C57BL6 X CBA/H) mice by collecting from oviducts 14h phCG (hours after injection of hCG) and washing in M2 medium containing 300 IU/ml hyaluronidase to remove cumulus cells. Subsequently, they were incubated in M2 containing 5 µg/ml cytochalasin B and placed in a chamber on the stage of an inverted microscope (Olympus IX70) equipped with micromanipulators (Narishige MO-188). The chromatin spindle (visualized under differential interference contrast) was aspirated as previously described<sup>51</sup>. ES cells CK35 derived from 129Sv/Pas blastocysts (generous gift from Pasteur Institute - Mouse Functional Genetics Unit) were used as donor cells. ES cell were synchronized in metaphase culture with 0.05 µg/ml of demecolcin for 2 hours. Cells were gently aspirated in and out of the injection pipette (inner diameter 7–8 µm) followed by microinjection into the cytoplasm of the enucleated oocytes with a Piezo<sup>51,52</sup>. NT embryos were activated by incubation for 3 h in Ca<sup>2+</sup>-free medium containing 10 mM Sr<sup>2+</sup>. Embryos with visible nuclei, considered as activated, were transferred into fresh M16 medium and cultured at 37°C in a humidified atmosphere containing 5% CO<sub>2</sub>. For microinjection embryos were placed in M2, in a chamber on the stage of a Nikon inverted microscope equipped with Narishige micromanipulators and an Eppendorf microinjector. Embryos were microinjected in the cytoplasm with 1-2 pl of the of the indicated mRNAs

(600 ng/μl for Suv39h1 or 250 ng/μl for Gfp or H2B-cherry). Microinjections were performed at 4-5 hours post-activation. Incubation was then carried out in M16 culture medium at 37°C, 5% CO<sub>2</sub> for further development.

### RNA-seq and library preparation

*For the suv39h1-injected pooled 2-cell stage analysis (Fig. 6a-b).* Control non-injected, Suv39h1wt or Suv39h1mut-injected embryos were collected at 46 hours post-hCG, washed in PBS and flash-frozen in Lysis Buffer from the Single-Cell Lysis Kit (Ambion 4458235). Duplicates of twenty embryos pooled from three independent experiments were acquired for each experimental group. Upon thawing embryos were subjected to DNase treatment, with 1μl DNase, incubated for 5 minutes at room temperature, then 1μl of Stop solution was added and incubated for 2 minutes, according to the manufacturer's instructions. Amplified cDNA was prepared from 2 ng of total RNA using the Ovation RNA-seq system V2 (NuGEN Technologies, Inc.) following manufacturer's instructions. Amplified cDNA was purified using AMPure XP beads (Beckman Coulter Inc.) and 500 ng were fragmented by sonication using a Covaris E210 instrument (with duty cycle: 10X, intensity: 5 and cycle/burst: 200 for 180 seconds). RNA-Seq Library preparation was performed using Ovation Ultralow Library System kit (NuGEN Technologies, Inc.) according to manufacturer's instructions. DNA libraries were checked using 2100 Bioanalyzer (Agilent) and quantified using Kapa Sybr Fast Light Cyclor 480 qPCR Kit (Kapa Biosystems). The libraries were loaded in the flow cell at 14pM concentration and sequenced in the Illumina HiSeq 2500. Image analysis and base calling were performed using RTA 1.18.61 and CASAVA 1.8.2.

*For dsSuv39h2-injected pooled 2-cell stage analysis (Fig. 3 c-d).* Embryos were cultured until 2-cell stage (42 h phCG) and pools of ten 2-cell stage embryos were washed with PBS, placed in tubes with 1x lysis buffer (Takara ST0948) and flash frozen in liquid nitrogen. RNA-seq was carried out with the SMART-seq2 protocol, as previously described<sup>53</sup> and subjected to paired-end sequencing on the Nextseq 500 (Illumina) platform. Notably, SMART-seq2, like all single-cell and low-input RNA-seq protocols available to date, relies on poly(A)-based amplification, and therefore our RNA-seq was unable to identify nonpolyadenylated and cryptic transcripts. We analyzed 4-6 biological replicates (pools of 5) for each experimental group. The numbers of replicates and reads per sample are indicated in Table S2.

*For Suv39h1 g.o.f. 2-cell stage to blastocyst single embryo analysis (Fig. 6c-d).* Embryos were cultured until the indicated timepoints post-hCG at which point a representative portion of embryos was collected. Collections were obtained from four independent experiments. Individual embryos were washed with PBS, placed in tubes with 1x lysis buffer (Takara ST0948) and flash frozen in liquid nitrogen. RNA-seq was carried out with the SMART-seq2 protocol<sup>53</sup> and subjected to paired-end sequencing on the Nextseq 500 (Illumina) platform. The numbers of replicates and reads per sample are indicated in Table S9.

### RNA-seq data analysis

*For the suv39h1-injected pooled 2-cell stage analysis ( Fig. 6a-b )* reads were mapped onto the mm9 assembly of the *Mus musculus* genome by using Tophat v2.0.14 (ref. 54) and the

bowtie v2-2.1.0 (ref. 55). Quantification of gene expression was performed using HTSeq v0.6.1 (ref. 56) and gene annotations from Ensembl release 67. Read counts were normalized across libraries as described (ref. 57) and data was analysed as described previously<sup>58</sup>, implemented in the DESeq2 Bioconductor library (DESeq2 v1.14.1). Resulting p-values were adjusted for multiple testing as described<sup>59</sup>. The following thresholds were used to select significantly differentially expressed (DE) genes (p-value adjusted for multiple testing < 0.05, |log<sub>2</sub> Fold-Change| > 1). Repeat analysis was performed as before<sup>25</sup>, by aligning reads to repetitive elements in two pass. In the first pass, reads were aligned to the non-masked *Mus musculus* reference genome (mm9) using BWA v0.6.2 (ref.60). Positions of the reads uniquely mapped to the *Mus musculus* genome were cross-compared with the positions of the repeats extracted from UCSC (rmsk table in UCSC database for *Mus musculus* mm9) and reads overlapping a repeat sequence were annotated with the repeat family. In the second pass, reads not mapped or multi-mapped to the *Mus musculus* genome in the previous pass were aligned to RepBase<sup>61</sup> v18.07 repeat sequences for Rodent. Reads mapped to a unique repeat family were annotated with the family name. Finally, we summed the read counts per repeat family of the two annotation steps. Data were normalized based on library size and data was analysed as implemented in the DESeq2 Bioconductor library (DESeq2 v1.14.1)<sup>58</sup>. p-values were adjusted for multiple testing using the Benjamini and Hochberg method.

*For dsSuv39h2 –injected pooled 2-cell stage analysis ( Fig. 3c-d ),* RNA-seq sequencing reads were trimmed using BBduk (<http://jgi.doe.gov/data-and-tools/bbtools>) with the following parameters: ktrim=r, k=23, mink=11, hdist=1, tbo, tpe. Trimmed reads were mapped to the GRCm38 *Mus musculus* reference genome using STAR (version 2.5.2b) with the following parameters: --outFilterType BySJout --outFilterScoreMinOverLread 0.3 --outFilterMatchNminOverLread 0 --outFilterMismatchNmax 33 --seedSearchStartLmax 12 --alignSJoverhangMin 15. HTSeq tool htseq-count (version 0.9.1) was used for read counting against the gene annotations downloaded from gencode (Release M12, GRCm38.p5) with reverse strand setting. DE analysis was performed using DESeq2 (version 1.18.1). Spike-in normalisation factor was calculated from ERCC spike-in mix using the remove unwanted variation strategy from RUVseq (version 1.12.0). To calculate the spike-in normalisation factor genes with less than 5 reads in at least two samples were discarded. DESeq2 was run with the design: spike-in normalisation factor + conditions. Genes with normalised counts lower than 2 in at least 4 samples were discarded from the differential expression analysis. One of the replicates from the RNAi-lacz condition was discarded from the analysis due to unexpected number of reads mapped to the ERCC spike-in and clustering outlier in the quality control analysis, indicating technical failure. Genes with an adjusted *P* value 0.05 were considered significantly differentially expressed. lfcShrink function from DESeq2 was used for visualization purposes. Differential repeat expression analysis was performed on reads remapped with STAR using the recommended parameters for Tetranscripts: --outFilterMultimapNmax 100 --winAnchorMultimapNmax 200. Ambiguously mapped reads were used for differential repeat expression analysis using Tetranscripts (version 2.0.3) with the following parameters: --stranded no --mode multi. Repeat annotations were downloaded from RepeatMasker (<http://www.repeatmasker.org/>)

and repeats with the same id were merged. Differential expression analysis was performed as described above using the count table generated from TETranscripts.

*For Suv39h1 g.o.f. 2-cell stage to blastocyst single embryo analysis ( Fig. 6c-d ),* reads were cleaned of adapters using Trimmomatic v0.38 (ref.62), then Kallisto v0.44.0 (ref.63) was used to align the reads to the mouse genome mm10 (GRCm38.p6). Quality control tests were carried out using the R packages Scater<sup>64</sup> and Single Cell Experiment, by comparing the library size and ERCC counts, deleting the outlier embryos. Genes with an average number of counts  $\geq 10$  were kept for subsequent analysis. Counts were normalized by RPKM using edgeR<sup>65</sup> and were used to plot a diffusion map with Destiny package<sup>66</sup>. Diffusion pseudotime was calculated measuring the distance of the embryos to the tip corresponding to the 2-cell stage. Pairwise differential gene expression analysis was done between the Non-Injected, Suv39h1mut and Suv39h1wt embryos, using the method implemented by DESeq2 v1.22.1 (ref. 58). A normality test of Shapiro-Wilk was done, as the distributions are not normal we performed a Wilcoxon test. DE genes between the Suv39h1mut and Suv39h1wt embryos expression in normal embryos was analysed using previously scRNA-Seq data<sup>22</sup>. A feature scaling normalization was used for visualization of data between stages.

### Targeted QPCR high-throughput gene expression analysis

Control non-injected, Gfp-only, Suv39h1wt or Suv39h1mut-injected embryos or dsSuv39h2, dsLacZ or non-injected embryos were washed in PBS and flash frozen in liquid nitrogen in 5  $\mu$ l 2x reaction buffer (CellsDirect™ One-Step qRT-PCR kit, 11753100, ThermoFisher) at 46 or 78 hours post-hCG for the 2-cell stage or morula-stage analyses respectively. TaqMan® Gene Expression Assays (20x Applied Biosystems), previously tested using ES cell cDNA for amplification efficiency, were pooled to a final concentration of 0.2x for each of the 45 assays. To each of the single-cell samples in 2x reaction buffer was added 2.5  $\mu$ l 0.2x assay pool, 0.5  $\mu$ l RT/Taq enzyme (CellsDirect™ One-Step qRT-PCR kit, 11753100, ThermoFisher) and 2.3  $\mu$ l of water. Cell lysis and sequence-specific reverse transcription were performed at 50°C for 20 minutes. The reverse transcriptase was inactivated by heating to 95°C for 2 minutes. Sequence-specific pre-amplification was performed by denaturing at 95°C for 15 seconds, then annealing and amplification at 60°C for 4 minutes for 18 cycles. The resulting cDNA was diluted 5-fold before analysis with Universal PCR Master Mix and TaqMan® Gene Expression Assays (Applied Biosystems) in 48:48 Dynamic Arrays on a Biomark™ System (Fluidigm). For the 2-cell stage analysis a DNase treatment was incorporated as Taqman® Gene Expression Assays targeting repetitive elements were utilized, immediately after cell lysis by incubation of the embryo in 4 $\mu$ l 2x reaction buffer with 2.5 $\mu$ l DNase and 0.7 $\mu$ l DNase buffer (CellsDirect™ One-Step qRT-PCR kit, 11753100, ThermoFisher) for 15 minutes at room temperature. The treatment was stopped by addition of 5mM EDTA and incubated for 10 minutes at 70°C. Subsequently 5 $\mu$ l of 2x reaction buffer, 0.4  $\mu$ l RT/Taq, 4.9 $\mu$ l of assay pool and 2.5 mM MgSO<sub>4</sub> were added and incubated for 20 minutes at 50°C for reverse transcription. The following steps were identical to the above, except a 10-fold dilution was carried out before qPCR analysis, due to the high expression of some targets (rDNAs, SINEs). Ct values were calculated from the system's software (Biomark™ Real-time PCR analysis, Fluidigm). All Raw Ct values were normalized to the

assumed detection Ct level of 28 following recommendation from Fluidigm technical support<sup>11</sup>. Ct values greater than 28 and those with curve qualities lower than 0.65 were deemed unreliable measurements and had their Ct values substituted with 28. Whenever Ct values or quality scores were judged unreliable in one replicate, but not in the other, those of the successful replicate were kept. Additionally, all samples lacking expression of reference genes Actin-b and Gapdh were removed from further analysis. The remaining Ct values were subtracted from 28 in order to achieve a scale where zero corresponds to the lack of expression and an increase of 1 unit indicates a doubling of the expression level<sup>11</sup>. Violin plots of the resulting dataset were generated using the ggplot2 R package. Statistical analysis was performed using the Mann-Whitney U test. For the Suv39h1 (Fig. 1a) and Suv39h2 (Fig. 1d) expression analysis during preimplantation development the detailed methods are described<sup>11</sup>. Data are presented as absolute expression values.

### Methyltransferase Assay

The pGEX-6P1/Suv39h1/FL/BC and pGEX-6P1/Suv39h2FL/477/BC and plasmids were constructed by inserting synthetic genes (Integrated DNA technologies), which were optimized with bacterial codons, coding for murine Suv39h1 and Suv39h2 into the pGEX-6P1 plasmid using EcoRI and XhoI restriction sites. Suv39h1 and Suv39h2 proteins were expressed in BL21 gold bacterial cells. Cells were grown in 2xYT medium containing 100µg/ml ampicillin, induced with 0,4 mM isopropyl-β-D-1-thiogalactopyranoside when OD600 was 0,8 overnight at 16°C, and harvested by centrifugation. Bacterial cells were lysed in a buffer containing 40mM Tris-HCl pH 8.0, 9% glycerol, 2,5 mg/ml and cOmplete, EDTA-free protease inhibitor cocktail tablets. Lysate was digested with 25U/ml benzonase, mixed with total 0,5M KCl, 0,1% NP40, 0,2% Tritonx100, sonicated (20 times 1s ON, 2s OFF) and centrifuged at 4°C, 12000xg for 30 min. Supernatants were affinity purified using Glutathione Sepharose 4B (purchased from GE Healthcare Life Sciences). In order to remove bacterial chaperones bound to the protein, after 2h and 45 minutes incubation of glutathione sepharose with lysate, 3 ml of supernatant was collected (per 0,5l starting culture), incubated 5 min at 70°C with rotation and then spun down at maximum speed for 1 min. Supernatant was mixed with the rest of sepharose-lysate suspension and 1mM of ATP and samples were incubated for 30 minutes. Glutathione sepharose was washed 3 times with 15 ml buffer containing 40mM Tris-HCl pH 8.0, 0,5M KCl, 9% glycerol, 0,1% Tritonx100, 0,1% NP40 and 3 times with 15 ml of the same buffer also containing 0,05mM ZnCl<sub>2</sub>. Proteins were eluted with buffer containing 20mM Tris-HCl pH 8.0, 0,5M KCl, 9% glycerol, 1mM DTT and 10mM reduced glutathione pH 8.0. For the histone methyltransferase assay, purified proteins were pre-incubated with dsRNA for 30 min at 4°C, mixed with 2,67 µM of recombinant histone H3.1, 6 µM hot 3H-SAM (1,5 µCi), and incubated for 30 min at 30°C. SDS-PAGE was performed on the reaction mixtures and subsequently transferred to PDV membrane. The membranes were stained with Amido Black and sprayed with enhancer and autoradiography film was exposed for 1h.

### MEF Cells

The Suv39h1/2 double knock-out MEF cells have previously been characterised<sup>10</sup>.

### H3K9me3 Chip-seq Analysis

Allele-specific H3K9me3 ChIP-seq signal tracks<sup>12</sup> were obtained as described<sup>67,68</sup> and normalized to input. H3K9me3 ChIP-seq has been extensively characterized in reference 12. Gene coordinates were obtained from Ensembl using Biomart and average ChIP-seq signal over the gene body was computed using BEDOPS' bedmap<sup>69</sup>. Heatmap was generated using deepTools. For the metagene plots in Fig. 3b, peaks were called using the Epic implementation of the SICER algorithm<sup>70</sup> and genes were classified depending on whether they overlapped an H3K9me3 peak exclusively in the paternal allele, exclusively in the maternal allele or in both alleles. We used the Epic implementation of the SICER algorithm because it is more appropriate for calling peaks at a broader domain. Since H3K9me3 localisation is usually rather broad, we consider SICER to be more appropriate than MACS2. For ChIP analysis in Fig. 3e, ChIP-seq sequencing reads obtained from SRA were trimmed using trim\_galore (version 0.5.0) with the --paired setting. Trimmed reads were mapped to the GRCm38 *Mus musculus* reference genome with bowtie2 (2.2.4) in paired-end mode using the --very-sensitive setting. ChIP-seq tracks were generated using macs2 (version 2.1.1) callpeak independently from the mapped input and signal reads. Fold-enrichment tracks normalised to input were generated using the bdgcmp tool on the resulting Bedgraph files for input and signal. DeepTools (version 3.0.1) was used to produce the heatmaps with flanking size of 5Kb upstream and down-stream of the TSS and a bin size of 10bp.

### Analysis of published RNA-seq data (Fig. 3f-g)

We used previous data<sup>22,71</sup> from GEO (GSE45719 and GSE38495). Single end reads were trimmed for adaptor sequences using trimmomatic 0.36 and mapped to the mm10 reference genome using STAR 2.5.3a and the GENCODE M13 annotation. RPKMs were computed through the HTSeq pipeline and detectable genes were defined as having a median expression in the single-cell expression dataset higher than zero. Plotting was performed using ggplot2.

### Analysis of published ATAC-seq data (Fig. 3h)

ATAC-seq data<sup>26</sup> was downloaded from GEO accession GSE66390. Paired end reads were trimmed for adaptor sequences using trimmomatic 0.36 and mapped to the mm10 reference genome using bowtie2 with parameters --dovetail -X 2000 --no-discordant --no-mixed. The resulting bam files were filtered for non-uniquely mapping reads using samtools with a MAPQ threshold of 10 and filtered for duplicates using Picard Tools' MarkDuplicates. Finally, mitochondrial reads were removed using samtools and signal tracks were generated using macs2.1.1 with parameters --SPMR--nomodel --nolambda--shift-100--extsize 200 for the combined reads of all replicates of the same population. Gene coordinates were obtained from Ensembl using Biomart and average ATAC-seq signal over the gene body was plotted using deepTools.

### Paternal H3K9me3 enrichment for transposable elements (Extended Data Fig. 3a-b)

Mapping was done as described<sup>12</sup> using the default multi-mapping strategy of bwa mem. Transposable element (TE) annotations were downloaded from Repeatmasker (<http://>

[repeatmasker.org/](http://repeatmasker.org/), version mm9 open-3.2.8). For the TE enrichment spectrum (Extended Data Fig. 3a) the genome was partitioned into 10kb bins. Bins were assigned and sorted by the average paternal H3K9me3 signal in that region. For each bin, we counted the number of TEs of a given type that lie within a particular bin (measured at the TE center). The resulting vector was then smoothed using a sliding window average of 1000 bins and normalised by dividing by its mean and subsequently log<sub>2</sub> transformed. Hence, negative values in the enrichment vector indicate depletion of TE copies in regions with a particular H3K9me3 average, positive values indicate enrichment. P-values were calculated using Mann-Whitney U test on the distribution of all average paternal H3K9me3 values in the binned non-smoothed genome vs. the distribution of values in bins that contained a copy of the given TE class and adjusted using the Bonferroni procedure. Only TEs with adjusted p-values < 0.01 are displayed in (Extended Data Fig. 3a). Each row in the spectrum plot corresponds to a single type of TE and columns are ordered by increasing H3K9me3 value (for clarity, all bins with H3K9me3 average equal to 0 were collapsed into a single column by calculating their average TE enrichment value). Rows were ordered by hierarchical clustering using the centroid linkage method. Enrichment meta-profiles for specific examples (Extended Data Fig. 3b) display the trimmed mean paternal H3K9me3 signal (red line; trimmed mean cut-off 0.05) in a 40kb window around all copies of a given TE class. For visual reference, meta-profile plots include a random profile (grey line) generated by randomly choosing the same number of genomic regions in the genome as TE copies (maintaining the number of copies per chromosome) and performing the same enrichment analysis on the random set of regions.

### NicE-seq for accessible chromatin analysis of mouse preimplantation embryos

Zygotes were cultured until the 8-cell stage (72h phCG). The zona pellucida was removed and 10x 8-cell stage were fixed in 1% PFA and quenched with 50 mM glycine. NicE-seq library was prepared using a modified protocol<sup>72</sup>. Libraries were made on streptavidin magnetic beads using the NEB Ultra II kit.

### NicE-seq data processing and peak calling

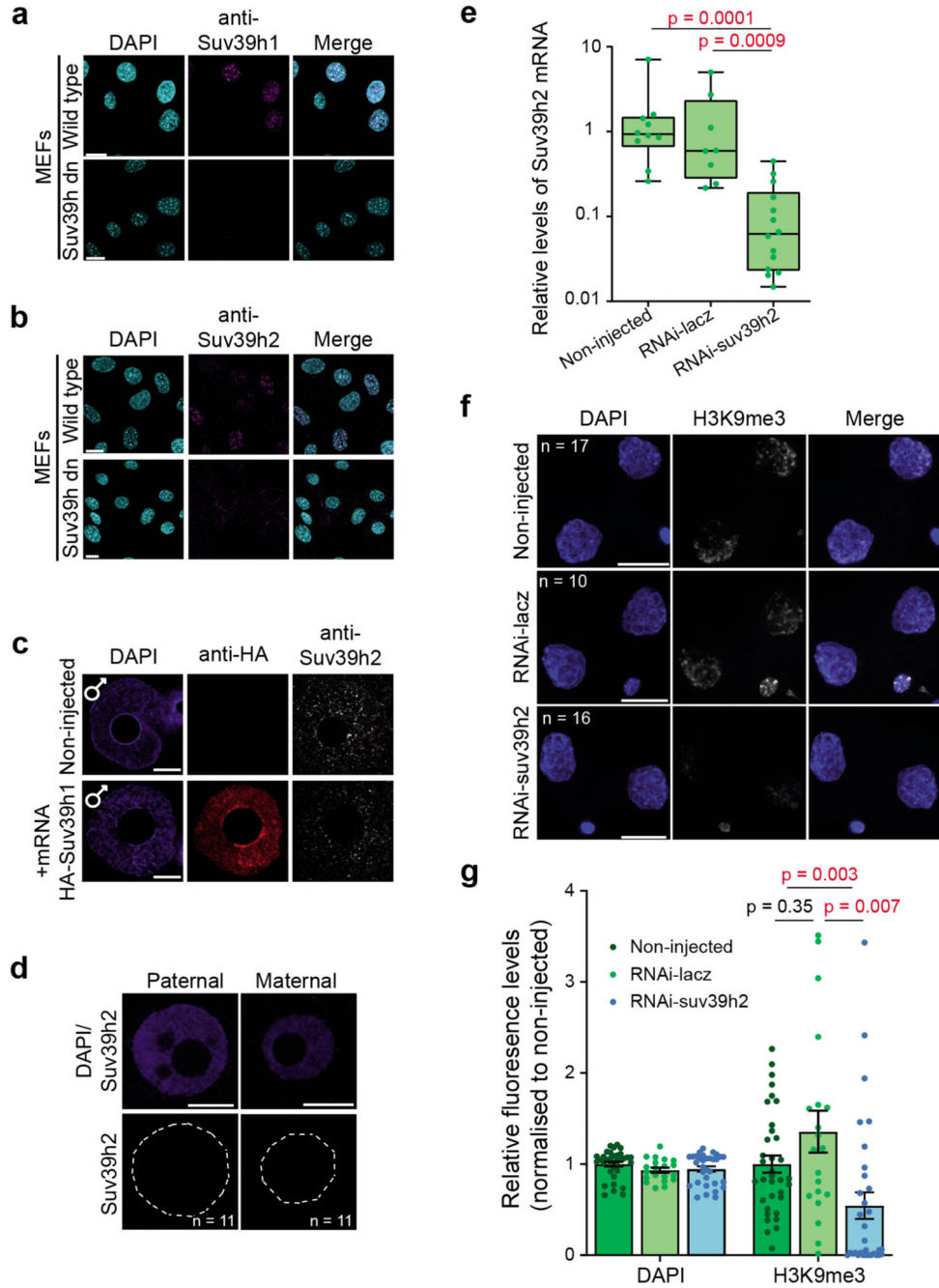
Adaptor and low-quality sequences were trimmed from paired-end sequencing reads using Trim Galore ([http://www.bioinformatics.babraham.ac.uk/projects/trim\\_galore/](http://www.bioinformatics.babraham.ac.uk/projects/trim_galore/)) with the following setting: `--clip_R1 4 --clip_R2 4 --three_prime_clip_R1 4 --three_prime_clip_R2 4`. Trimmed read pairs were mapped to the reference genome (mouse: mm10) using Bowtie2 (ref. 73) with the following arguments: `--dovetail --no-unal --no-mixed --no-discordant --very-sensitive-I 0 -X 1000`. Further, PCR duplicates and mitochondrial reads were removed using Picard tools and samtools respectively. Properly aligned read pairs were used for peak calling with MACS2 (ref.74) using `'macs2 callpeak -f BAMPE,--nolambda,--nomodel` options. The Fraction of reads in peaks (FRiP) score was calculated using the deepTools `plotEnrichment` function<sup>75</sup>. Peaks from the biological replicates were merged together using the `Bedtools`<sup>76</sup>. Peaks called from S and L samples were compared using the `Bedtools` and `mergepeaks.pl` command of Homer. First peaks from all the samples are concatenated. Peaks that have at least one base pair overlapping are considered associated and are merged to form a union peak set. Then peaks of individual samples were compared to the union set and were marked as either “unique” or “common”. Last the numbers of “unique” and “common”

peaks were summarized from all the samples and were used to make Venn Diagrams in R. NicE-Seq peaks were annotated using HOMER annotatePeaks.pl. HOMER annotates peaks as promoter (i.e., within 2 kb of known TSS), intergenic, intronic, exon, CpG islands, repetitive elements and other positional categories. Signal tracks were generated using 100bp bins using deeptools bamCoverage with the following parameters: --of bigwig --normalizeUsing RPKM.

### Statistics and Reproducibility

Statistical tests were performed minding data distribution and taking into consideration the number of data points available. Details on sample sizes, in addition to the statistical tests conducted, are shown on the corresponding figure legends. The normality of the distributions was tested using the Kolmogorov-Smirnov test. If the data was found not to be normally distributed, the non-parametric two-tailed Mann-Whitney U-test was used, otherwise the unpaired students t-test was used. The experiments throughout the manuscript were reproduced successfully across the indicated number of experiments, as reported in the figure legends. In the case on Fig. 2c seven independent experiments with Suv39h1 and nine independent experiments with Suv39h2 were performed. In 5 out of the 7 experiments with Suv39h1, a modest upregulation of KMT activity was observed (as represented by the Figure) and never any downregulation. By contrast, in 4 out of the 9 experiments with Suv39h2, a downregulation was observed (as represented by the Figure).

## Extended Data



**Extended Data Fig. 1. De novo H3K9me3 activity occurs immediately after fertilization**  
**a-b.** Wild-type and Suv39h1/2 double knock-out MEF cells immunostained with a anti-Suv39h1 and b anti-Suv39h2 antibody. Shown is a representative single confocal section from 2 independent experiments. Scale bar 20  $\mu$ m.  
**c.** Zygotes microinjected with HA-Suv39h1 mRNA as described in Fig.4a were fixed and immunostained with anti-HA and anti-Suv39h2 antibodies after 8 hours. A representative single confocal section of the paternal pronucleus in 7 zygotes from 2 independent

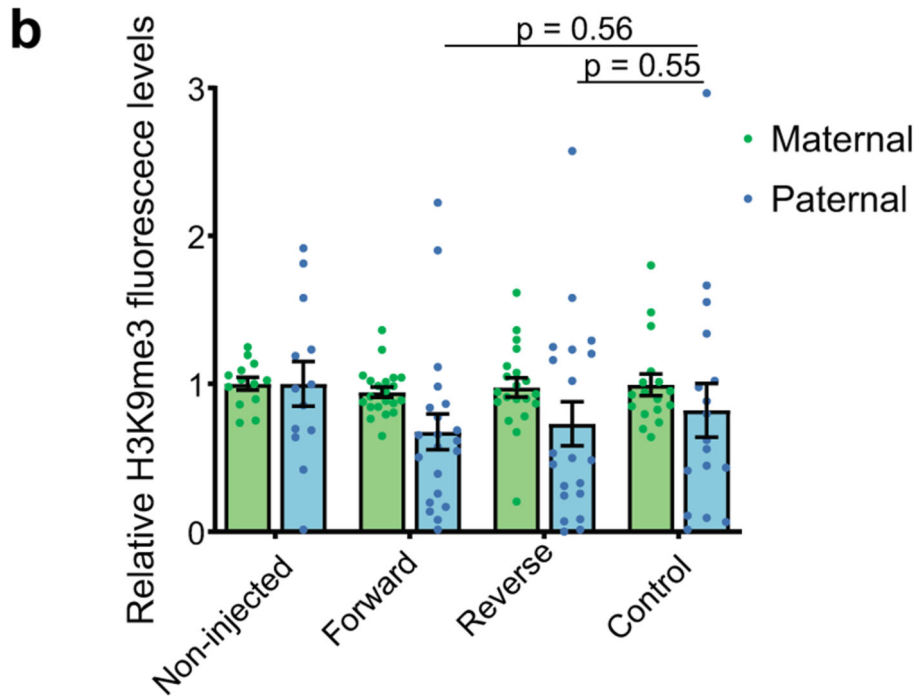
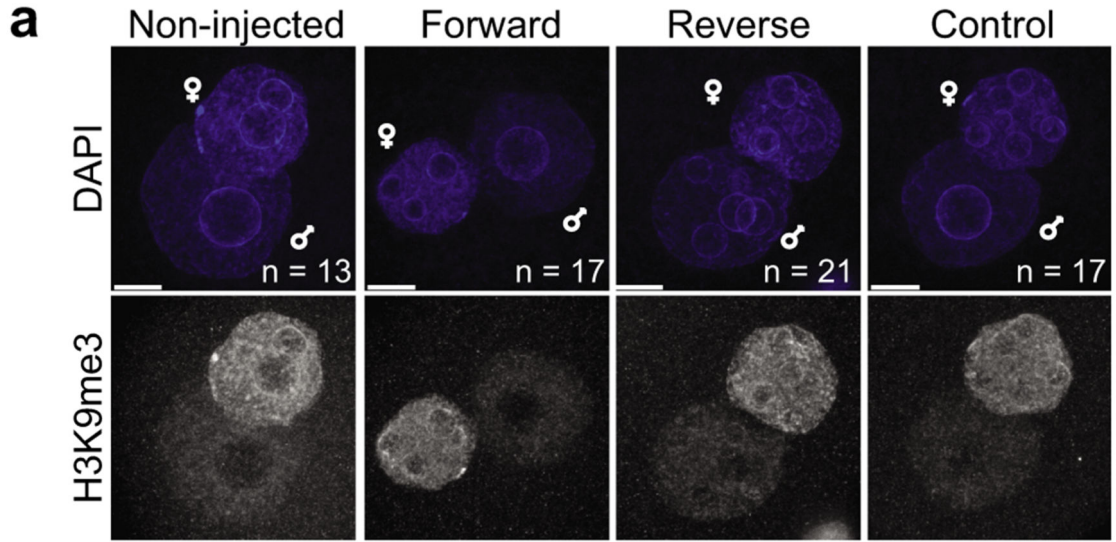
experiments is shown. The anti-Suv39h2 antibody does not recognise Suv39h1 protein. Scale bar 10  $\mu\text{m}$ .

**d.** Suv39h2 immunostaining in the two pronuclei in the early zygote (19 hours post-hCG). Shown is a representative embryo of 11 from 3 independent experiments.

**e.** Knockdown efficiency of dsRNA targeting Suv39h2 was assessed by RT-qPCR of Suv39h2 mRNA at 30h post-hCG in single embryos, the same timing as the immunofluorescence experiments shown in Fig.1g-h. The data represents the average fold change of Suv39h2 levels normalized to average levels of Actin-b and Gapdh in each embryo. N = the indicated number of embryos across 3 independent experiments. The box plots depict the median and interquartile range. The two sided Mann-Whitney U-test was used to compare experimental groups.

**f.** Representative maximum intensity projections of 2-cell stage embryos upon Suv39h2 RNAi using dsRNA, immunostained with anti-H3K9me3 antibodies. N = total number of individual embryos analysed in each group across 3 independent experiments for Suv39h2 and 2 for control knockdown. Scale bar 10  $\mu\text{m}$ .

**g.** Quantification of average fluorescence intensity for H3K9me3 in 2-cell stage nuclei. Data were normalized to the average H3K9me3 signal in non-injected embryos and are presented as mean  $\pm$  S.E.M (n = as in f). Statistical analysis was performed using the two-sided Mann-Whitney U test for comparing nonparametric distributions. Statistical source data are shown in Source data extended data fig. 1.

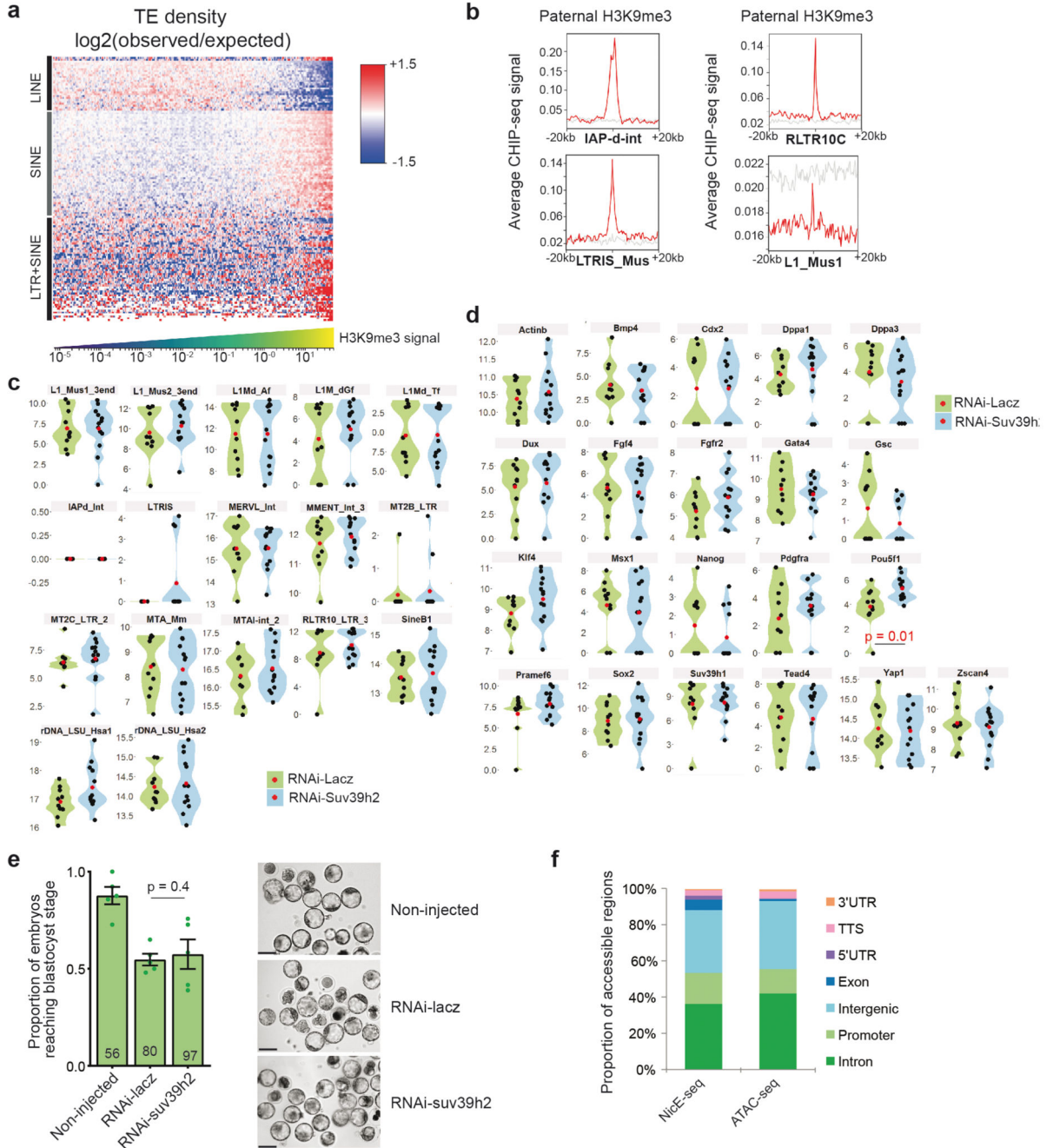


**Extended Data Fig. 2. RNA modulation of the KMT activity of Suv39h2 attenuates H3K9me3 levels in the early preimplantation mouse embryo**

**a.** Representative full z-series projections of confocal stacks of the indicated number of embryos manipulated as described in Figure 2d, injected instead with single-stranded forward or reverse major satellite transcripts from 2 independent experiments. Paternal and maternal pronuclei are indicated. Scale bar 10  $\mu$ m.

**b.** Quantification of the levels of H3K9me3 staining in the maternal and paternal pronuclei across embryos represented in a. Maternal and paternal H3K9me3 levels were normalized to

average levels in non-injected embryo. The graph depicts the mean  $\pm$  S.E.M. (n = the number of embryos analysed as indicated in a across 2 independent experiments). Statistical analysis was performed using the two-sided Mann-Whitney U test for comparing nonparametric distributions. Statistical source data are shown in Source data extended data fig. 2.



Extended Data Fig. 3. H3K9me3 is compatible with gene expression during early preimplantation development

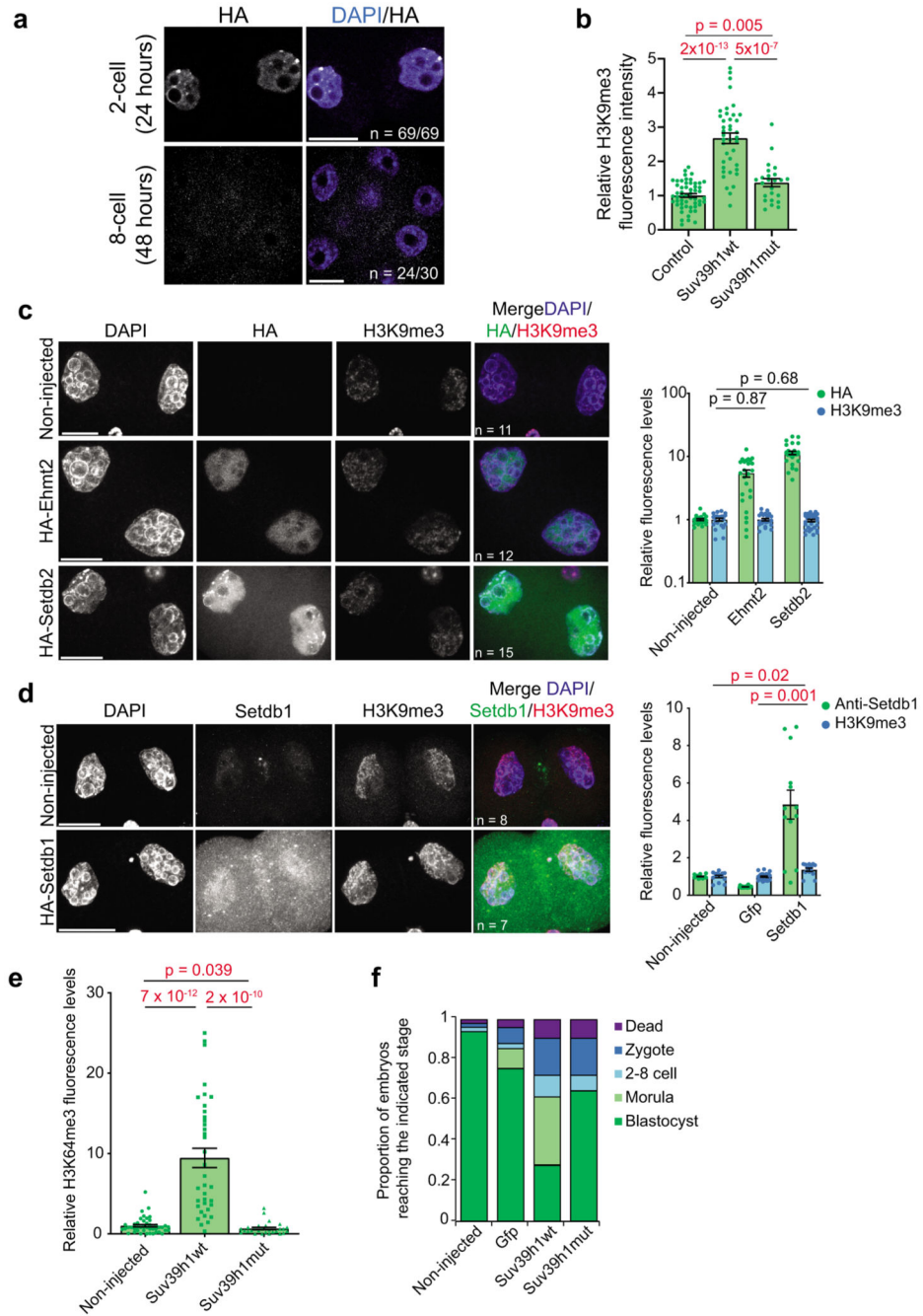
**a.** Enrichment heatmap ( $\log_2$  observed/expected TE density) in regions with differing paternal H3K9me3 levels. Columns correspond to 10kb binned genomic regions sorted from left to right by increasing H3K9me3 levels. Rows correspond to individual TE types hierarchically clustered using the centroid linkage method. Clusters are coarsely annotated with the dominant TE families. H3K9me3 ChIPseq data from<sup>12</sup> was reanalyzed for panels a and b.

**b.** Examples of paternal H3K9me3 levels in a 40kb region around selected TE classes (red line, 5% trimmed mean; grey, randomized signal).

**c-d.** Violin plots showing relative expression values of the indicated repetitive elements (c) or genes (d) in knockdown of Suv39h2 against control (LacZ) knockdown embryos at the 2-cell stage (46h post-hCG). The mean expression value of  $n = 10$  embryos (control) and  $n = 13$  embryos (Suv39h2 knockdown) from 3 independent experiments is depicted as a red point and the individual expression in each embryo as black dots. Statistical analysis was performed using the two-sided Mann-Whitney U test. See Table S4 for a list of genes (sheet1), REs (sheet2), and for the genes Taqman® assay IDs and reason(s) for inclusion.

**e.** Shown is the mean ( $\pm$  S.E.M.) proportion of embryos that reached the blastocyst stage 3 days after microinjection ( $n$  = the total number of embryos analysed is indicated from 5 independent experiments). Statistical analysis was performed using the N-1 Chi-squared test for comparing independent proportions. On the right are shown representative brightfield images of embryos. Images were taken at 120h post-hCG injection. Scale bar 100  $\mu\text{m}$ .

**f.** Comparison of the genomic distribution of open chromatin identified by NicE-seq compared to ATAC-seq in 8-cell stage mouse preimplantation embryos. Statistical source data are shown in Source data extended data fig. 3.



#### Extended Data Fig. 4. Suv39h1 induces constitutive heterochromatin

- a.** Zygotes were microinjected with HA-Suv39h1 mRNA, cultured for 24 or 48 hours, fixed and immunostained with an anti-HA antibody. A representative full z-series projection from at least 3 independent experiments is shown. Scale bar 10  $\mu$ m.
- b.** Mean levels of H3K9me3 ( $\pm$ S.E.M) in 2-cell embryos (42-44h post-hCG). Confocal stacks were reconstructed with IMARIS and nuclei were segmented using the DAPI channel. Fluorescence intensity was quantified in each nucleus after background subtraction. N =

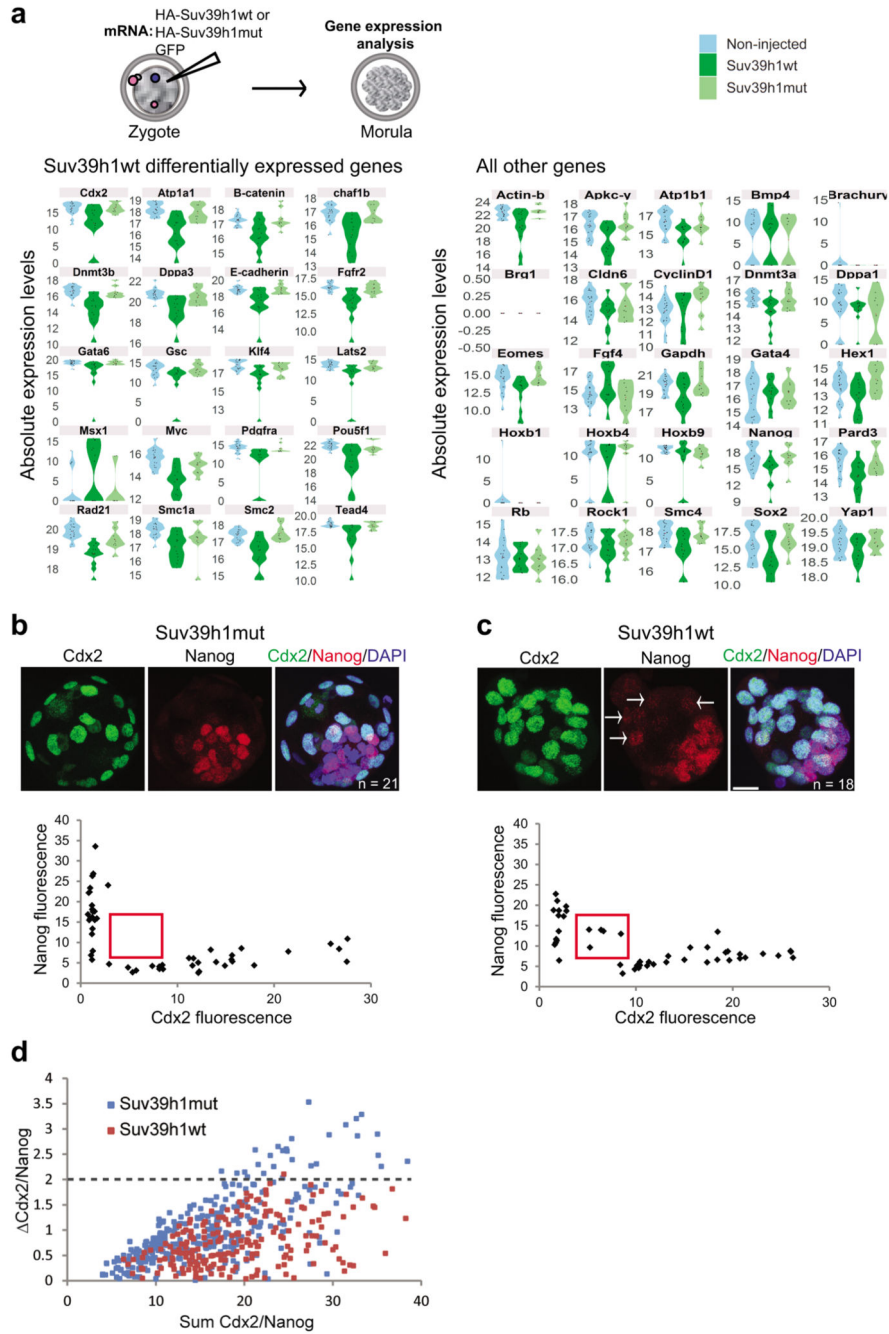
numbers as in Fig.4d. Statistical analysis was performed using the two-sided Mann-Whitney U test.

**c.** Zygotes were microinjected with Ehmt2 (G9a) or Setdb2 mRNA, fixed at the 2-cell stage (42-44h post-hCG) and immunostained with anti-H3K9me3 and anti-HA antibodies. A representative full z-series projection is shown. Mean fluorescence levels ( $\pm$  S.E.M.) are shown on the right (n = the total number of embryos analysed as indicated on the left panels across 2 independent experiments). Statistical analysis was performed using the Mann-Whitney U test. Scale bar 20  $\mu$ m.

**d.** As in c but with Setdb1 mRNA. Mean fluorescence levels ( $\pm$  S.E.M.) are shown on the right (n = the total number of embryos analysed as indicated on the left panels across 2 independent experiments). Statistical analysis was performed using the two-sided T test. Scale bar 20  $\mu$ m.

**e.** Mean levels ( $\pm$  S.E.M) of H3K64me3 in 2-cell stage embryos (42-44 hours post-hCG injection) after Suv39h1wt or Suv39h1mut expression. N = total number of embryos analysed is show in fig. 4h across 5 independent experiments for Suv39h1wt and 4 for Suv39h1mut. Statistical analysis was performed using the two-sided Mann-Whitney U test.

**f.** Summary of the stages of development for which embryos arrested as described in Fig.5b. N = numbers as in fig. 5b. Statistical source data are shown in Source data extended data fig. 4.

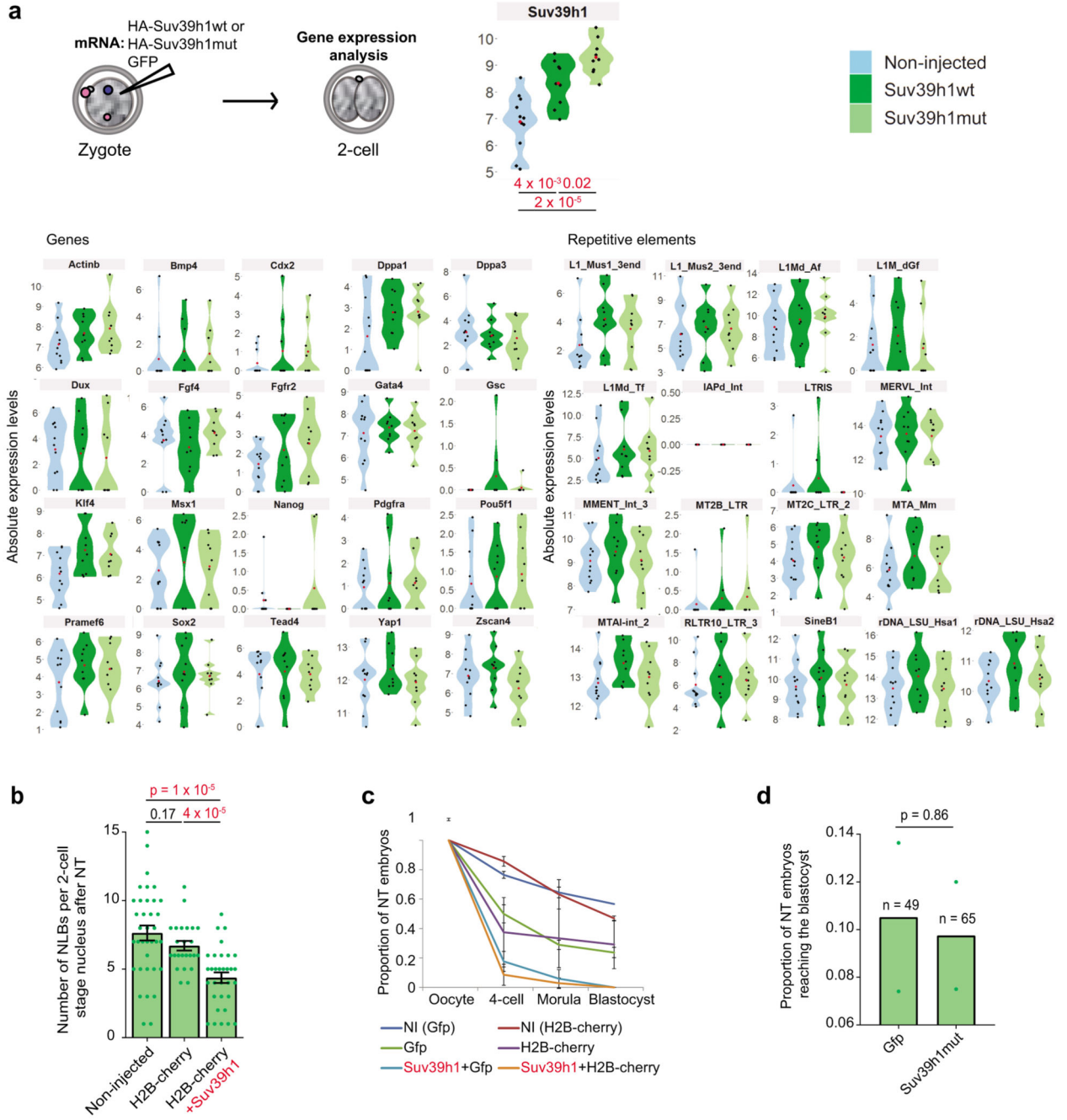


**Extended Data Fig. 5. Suv39h1 compromises development**

**a.** Violin plots depicting absolute expression levels (log<sub>2</sub> scale) in single Suv39h1wt, Suv39h1mut-expressing embryos and non-injected controls at the morula stage (78 hours post-hCG). Expression values in individual embryos are indicated by black points and the mean by a red point. Genes with a significant difference ( $P < 0.05$ ; two-sided Mann-Whitney U test) between the Suv39h1wt group and both control groups are shown on the left.  $N =$  numbers and stages of the embryos acquired from 3 independent experiments are shown in Table S5 and a list of genes analysed are shown in Table S6.

**b-c.** Embryos injected with mRNA encoding Suv39h1mut (control) or (c) Suv39h1wt were cultured to the blastocyst stage, fixed and immunostained with the indicated antibodies. Shown are representative full z-series projections. N = number of embryos analyzed from 2 independent experiments is indicated. Scale bar 20  $\mu\text{m}$ . Arrows in Nanog panel in c indicate cells ectopically expressing low levels of NANOG. The graphs below show the levels of NANOG and CDX2 in individual nuclei, for the representative embryos above. A clear segregation of CDX2 or NANOG positive populations is apparent in the controls, but is less pronounced in the Suv39h1wt-injected embryos. The red box indicates a consistent population of double CDX2/NANOG positive cells present in Suv39h1wt embryos only.

**d.** The absolute difference in intensity ( $\text{Cdx2/Nanog}$ ) for each nucleus (plotted points) from the embryos classified as blastocysts ( $>32$  cells) plotted against the sum of the NANOG and CDX2 signal ( $n = 7$  embryos for Suv39h1mut and 5 for Suv39h1wt across 2 independent experiments). Fewer nuclei have high  $\text{Cdx2/Nanog}$  and more nuclei have high sum  $\text{Cdx2/Nanog}$  scores in the Suv39h1wt embryos, suggesting a defect in the resolution of the outer and inner lineages. Statistical source data are shown in Source data extended data fig. 5.



**Extended Data Fig. 6. Suv39h1 inhibits epigenetic reprogramming**

**a.** Violin plots depicting absolute expression levels in log2 scale in single Suv39h1wt, Suv39h1mut-expressing embryos and non-injected controls at the late 2-cell stage (46 hours post-hCG). N = 9, 9 and 11 single embryos respectively across 3 independent experiments. Expression values in individual embryos are indicated by black points and the mean by a red point. The only gene or RE displaying significant difference using the two-sided Mann-Whitney U test between groups is Suv39h1 itself. See Table S4 for a list of genes (sheet1), REs (sheet2), and for the genes Taqman® assay IDs and reason(s) for inclusion.

**b.** The mean number of nucleolar-like bodies (NLBs) ( $\pm$  S.E.M.) inside each 2-cell stage nucleus from confocal stacks of DAPI stained embryos was counted manually ( $n$  = the number of embryos analyzed is indicated across 4 independent experiments). Nuclear transfer embryos were fixed at 25 and 33 hours post-activation with similar results obtained at the two time points. Statistical testing was performed using the two-sided Mann-Whitney U test for comparing nonparametric distributions.

**c.** Shown is a summary of the developmental progression of nuclear transfer embryos microinjected with the indicated mRNAs according to the workflow in Fig.7a. Developmental progression was monitored daily and the proportion of embryos that reached each stage of development was calculated. The data represents the mean ( $\pm$ S.E.M) ( $n$  = the total number of embryos analysed as indicated in Fig.7c across 3 independent experiments except for H2B-cherry alone, which was done twice).

**d.** The mean proportion of embryos injected with Suv39h1mut or GFP developing to the blastocyst stage is shown.  $N$  = the number of embryos tested across 2 independent experiments is indicated on the graph. Statistical analysis was performed using the N-1 Chi-squared test for comparing independent proportions. Statistical source data are shown in Source data extended data fig. 6.

## Supplementary Material

Refer to Web version on PubMed Central for supplementary material.

## Acknowledgments

We thank A.J. Bannister for providing the Suv39h1 cDNA and S. Daujat for providing the H3K64me3 antibody, K. Swist for help with expression of recombinant Suv39h enzymes and analysis of data shown in Figure 2C., A.J. Bannister and members of the IES for helpful discussions. We thank A. Ettinger for help with the blind counting and microscopy. C.G. and T.J. were supported by funds from the Max Planck Society. AE was partially funded through a MENRT fellowship. M.E.T.-P. acknowledges funding from EpiGeneSys NoE, ERC-Stg 'NuclearPotency', EMBO Young Investigator Programme, the Schlumberger Foundation for Research and Education and the Helmholtz Association and by the Deutsche Forschungsgemeinschaft (DFG, German Research Foundation) Project-ID 213249687 – SFB 1064. N.B and V.B were funded through the Laboratoire d'Excellence REVIVE (Investissement d'Avenir, ANR-10-LABX-73) and the INRA animal facilities (IERP, Jouy-en-Josas, France). J.M.V acknowledges funding from EpiGeneSys NoE and the Max Planck Society and S. G. from the Ministry of Science and Technology of China (grant number 2016YFA0100400).

## Data Availability

Sequencing data generated during this study have been deposited in the Gene Expression Omnibus (GEO) under accession codes GSE126021 (single-embryo RNA-seq for Suv39h1wt from 2-cell to morula stage); GSE126185 (RNA-seq for pooled Suv39h1-overexpressing embryos at 2-cell stage); GSE126492 (RNA-seq for pooled embryos with RNAi-Suv39h2 at 2-cell stage), GSE138686 (NicE-seq for embryos with RNAi-Suv39h2 at 8-cell stage).

Previously published mouse embryo datasets re-analysed here are available under accession codes GSE45719 and GSE38495 (single cell RNA-Seq); GSE66390 (ATACseq) and GSE98149 (H3K9me3 ChIP-seq).

All other data supporting the findings of this study are available from the corresponding author on reasonable request.

## Code Accessibility

All NGS data were analysed with standard programs and packages, as detailed in the Methods section. Code is available on request.

## References

1. Arney KL, Bao S, Bannister AJ, Kouzarides T, Surani MA. Histone methylation defines epigenetic asymmetry in the mouse zygote. *Int J Dev Biol.* 2002; 46:317–320. [PubMed: 12068953]
2. Burton A, Torres-Padilla ME. Chromatin dynamics in the regulation of cell fate allocation during early embryogenesis. *Nat Rev Mol Cell Biol.* 2014; 15:723–734. [PubMed: 25303116]
3. Santos F, Peters AH, Otte AP, Reik W, Dean W. Dynamic chromatin modifications characterise the first cell cycle in mouse embryos. *Dev Biol.* 2005; 280:225–236. [PubMed: 15766761]
4. Puschendorf M, et al. PRC1 and Suv39h specify parental asymmetry at constitutive heterochromatin in early mouse embryos. *Nat Genet.* 2008; 40:411–420. [PubMed: 18311137]
5. Santenard A, Torres-Padilla ME. Epigenetic reprogramming in mammalian reproduction: contribution from histone variants. *Epigenetics.* 2009; 4:80–84. [PubMed: 19242119]
6. Daujat S, et al. H3K64 trimethylation marks heterochromatin and is dynamically remodeled during developmental reprogramming. *Nat Struct Mol Biol.* 2009; 16:777–781. [PubMed: 19561610]
7. Wongtawan T, Taylor JE, Lawson KA, Wilmot I, Pennings S. Histone H4K20me3 and HP1alpha are late heterochromatin markers in development, but present in undifferentiated embryonic stem cells. *Journal of cell science.* 2011; 124:1878–1890. [PubMed: 21576353]
8. Bulut-Karslioglu A, et al. Suv39h-dependent H3K9me3 marks intact retrotransposons and silences LINE elements in mouse embryonic stem cells. *Mol Cell.* 2014; 55:277–290. [PubMed: 24981170]
9. Lachner M, O'Carroll D, Rea S, Mechtler K, Jenuwein T. Methylation of histone H3 lysine 9 creates a binding site for HP1 proteins. *Nature.* 2001; 410:116–120. [PubMed: 11242053]
10. Peters AH, et al. Loss of the Suv39h histone methyltransferases impairs mammalian heterochromatin and genome stability. *Cell.* 2001; 107:323–337. [PubMed: 11701123]
11. Burton A, et al. Single-Cell Profiling of Epigenetic Modifiers Identifies PRDM14 as an Inducer of Cell Fate in the Mammalian Embryo. *Cell Rep.* 2013
12. Wang C, et al. Reprogramming of H3K9me3-dependent heterochromatin during mammalian embryo development. *Nat Cell Biol.* 2018; 20:620–631. [PubMed: 29686265]
13. Burton A, Torres-Padilla ME. Epigenetic reprogramming and development: a unique heterochromatin organization in the preimplantation mouse embryo. *Brief Funct Genomics.* 2010
14. O'Carroll D, et al. Isolation and characterization of Suv39h2, a second histone H3 methyltransferase gene that displays testis-specific expression. *Molecular and cellular biology.* 2000; 20:9423–9433. [PubMed: 11094092]
15. Velazquez Camacho O, et al. Major satellite repeat RNA stabilize heterochromatin retention of Suv39h enzymes by RNA-nucleosome association and RNA:DNA hybrid formation. *Elife.* 2017; 6
16. Johnson WL, et al. RNA-dependent stabilization of SUV39H1 at constitutive heterochromatin. *Elife.* 2017; 6
17. Shirai A, et al. Impact of nucleic acid and methylated H3K9 binding activities of Suv39h1 on its heterochromatin assembly. *Elife.* 2017; 6
18. Maison C, et al. Higher-order structure in pericentric heterochromatin involves a distinct pattern of histone modification and an RNA component. *Nat Genet.* 2002; 30:329–334. [PubMed: 11850619]
19. Probst AV, et al. A strand-specific burst in transcription of pericentric satellites is required for chromocenter formation and early mouse development. *Dev Cell.* 2010; 19:625–638. [PubMed: 20951352]

20. Santenard A, et al. Heterochromatin formation in the mouse embryo requires critical residues of the histone variant H3.3. *Nat Cell Biol.* 2010; 12:853–862. [PubMed: 20676102]
21. Miyanari Y, Ziegler-Birling C, Torres-Padilla ME. Live visualization of chromatin dynamics with fluorescent TALEs. *Nat Struct Mol Biol.* 2013
22. Deng Q, Ramskold D, Reinius B, Sandberg R. Single-cell RNA-seq reveals dynamic, random monoallelic gene expression in mammalian cells. *Science.* 2014; 343:193–196. [PubMed: 24408435]
23. Wu J, et al. The landscape of accessible chromatin in mammalian preimplantation embryos. *Nature.* 2016; 534:652–657. [PubMed: 27309802]
24. Probst AV, Santos F, Reik W, Almouzni G, Dean W. Structural differences in centromeric heterochromatin are spatially reconciled on fertilisation in the mouse zygote. *Chromosoma.* 2007; 116:403–415. [PubMed: 17447080]
25. Fadloun A, et al. Chromatin signatures and retrotransposon profiling in mouse embryos reveal regulation of LINE-1 by RNA. *Nat Struct Mol Biol.* 2013; 20:332–338. [PubMed: 23353788]
26. Eid A, Rodriguez-Terrones D, Burton A, Torres-Padilla ME. SUV4-20 activity in the preimplantation mouse embryo controls timely replication. *Genes Dev.* 2016; 30:2513–2526. [PubMed: 27920088]
27. Schultz RM. The molecular foundations of the maternal to zygotic transition in the preimplantation embryo. *Hum Reprod Update.* 2002; 8:323–331. [PubMed: 12206467]
28. Surani MA, Hayashi K, Hajkova P. Genetic and epigenetic regulators of pluripotency. *Cell.* 2007; 128:747–762. [PubMed: 17320511]
29. Matoba S, et al. Embryonic development following somatic cell nuclear transfer impeded by persisting histone methylation. *Cell.* 2014; 159:884–895. [PubMed: 25417163]
30. Ribeiro-Mason K, et al. Nuclear dynamics of histone H3 trimethylated on lysine 9 and/or phosphorylated on serine 10 in mouse cloned embryos as new markers of reprogramming? *Cell Reprogram.* 2012; 14:283–294. [PubMed: 22775512]
31. Liu H, Kim JM, Aoki F. Regulation of histone H3 lysine 9 methylation in oocytes and early preimplantation embryos. *Development.* 2004; 131:2269–2280. [PubMed: 15102709]
32. Ogura A, Inoue K, Wakayama T. Recent advancements in cloning by somatic cell nuclear transfer. *Philos Trans R Soc Lond B Biol Sci.* 2013; 368
33. Martin C, et al. Architectural reorganization of the nuclei upon transfer into oocytes accompanies genome reprogramming. *Mol Reprod Dev.* 2006; 73:1102–1111. [PubMed: 16736527]
34. Hemberger M, Dean W, Reik W. Epigenetic dynamics of stem cells and cell lineage commitment: digging Waddington's canal. *Nat Rev Mol Cell Biol.* 2009; 10:526–537. [PubMed: 19603040]
35. Smith ZD, et al. A unique regulatory phase of DNA methylation in the early mammalian embryo. *Nature.* 2012; 484:339–344. [PubMed: 22456710]
36. Rea S, et al. Regulation of chromatin structure by site-specific histone H3 methyltransferases. *Nature.* 2000; 406:593–599. [PubMed: 10949293]
37. Nicetto D, et al. H3K9me3-heterochromatin loss at protein-coding genes enables developmental lineage specification. *Science.* 2019; 363:294–297. [PubMed: 30606806]
38. Wei J, et al. KDM4B-mediated reduction of H3K9me3 and H3K36me3 levels improves somatic cell reprogramming into pluripotency. *Sci Rep.* 2017; 7:7514. [PubMed: 28790329]
39. Onder TT, et al. Chromatin-modifying enzymes as modulators of reprogramming. *Nature.* 2012; 483:598–602. [PubMed: 22388813]
40. Soufi A, Donahue G, Zaret KS. Facilitators and impediments of the pluripotency reprogramming factors' initial engagement with the genome. *Cell.* 2012; 151:994–1004. [PubMed: 23159369]
41. Antony J, Oback F, Chamley LW, Oback B, Laible G. Transient JMJD2B-mediated reduction of H3K9me3 levels improves reprogramming of embryonic stem cells into cloned embryos. *Mol Cell Biol.* 2013; 33:974–983. [PubMed: 23263990]
42. Liu W, et al. Identification of key factors conquering developmental arrest of somatic cell cloned embryos by combining embryo biopsy and single-cell sequencing. *Cell Discov.* 2016; 2:16010. [PubMed: 27462457]

43. Hatanaka Y, et al. Histone chaperone CAF-1 mediates repressive histone modifications to protect preimplantation mouse embryos from endogenous retrotransposons. *Proc Natl Acad Sci U S A*. 2015; 112:14641–14646. [PubMed: 26546670]
44. Zyllicz JJ, et al. G9a regulates temporal preimplantation developmental program and lineage segregation in blastocyst. *Elife*. 2018; 7
45. Hanna CW, et al. MLL2 conveys transcription-independent H3K4 trimethylation in oocytes. *Nat Struct Mol Biol*. 2018; 25:73–82. [PubMed: 29323282]
46. Zhang B, et al. Allelic reprogramming of the histone modification H3K4me3 in early mammalian development. *Nature*. 2016; 537:553–557. [PubMed: 27626382]
47. Tsuroula K, et al. Temporal and Spatial Uncoupling of DNA Double Strand Break Repair Pathways within Mammalian Heterochromatin. *Mol Cell*. 2016; 63:293–305. [PubMed: 27397684]
48. Lehnertz B, et al. Suv39h-mediated histone H3 lysine 9 methylation directs DNA methylation to major satellite repeats at pericentric heterochromatin. *Curr Biol*. 2003; 13:1192–1200. [PubMed: 12867029]
49. Torres-Padilla ME, Bannister AJ, Hurd PJ, Kouzarides T, Zernicka-Goetz M. Dynamic distribution of the replacement histone variant H3.3 in the mouse oocyte and preimplantation embryos. *Int J Dev Biol*. 2006; 50:455–461. [PubMed: 16586346]
50. Jachowicz JW, Santenard A, Bender A, Muller J, Torres-Padilla ME. Heterochromatin establishment at pericentromeres depends on nuclear position. *Genes Dev*. 2013; 27:2427–2432. [PubMed: 24240232]
51. Zhou Q, Jouneau A, Brochard V, Adenot P, Renard JP. Developmental potential of mouse embryos reconstructed from metaphase embryonic stem cell nuclei. *Biol Reprod*. 2001; 65:412–419. [PubMed: 11466208]
52. Brochard V, Liu Z. Nuclear transfer in the mouse. *Methods Mol Biol*. 2015; 1222:1–14. [PubMed: 25287334]
53. Picelli S, et al. Smart-seq2 for sensitive full-length transcriptome profiling in single cells. *Nat Methods*. 2013; 10:1096–1098. [PubMed: 24056875]
54. Trapnell C, Pachter L, Salzberg SL. TopHat: discovering splice junctions with RNA-Seq. *Bioinformatics*. 2009; 25:1105–1111. [PubMed: 19289445]
55. Langmead B, Salzberg SL. Fast gapped-read alignment with Bowtie 2. *Nat Methods*. 2012; 9:357–359. [PubMed: 22388286]
56. Anders S, Pyl PT, Huber W. HTSeq – A Python framework to work with high-throughput sequencing data. *bioRxiv*. 2014
57. Anders S, Huber W. Differential expression analysis for sequence count data. *Genome Biol*. 2010; 11:R106. [PubMed: 20979621]
58. Love MI, Huber W, Anders S. Moderated estimation of fold change and dispersion for RNA-Seq data with DESeq2. *Genome Biol*. 2014; 15:550. [PubMed: 25516281]
59. Benjamini Y, Hochberg Y. Controlling the False Discovery Rate: A Practical and Powerful Approach to Multiple Testing. *Journal of the Royal Statistical Society*. 1995; 57:289–300.
60. Li H, Durbin R. Fast and accurate short read alignment with Burrows-Wheeler transform. *Bioinformatics*. 2009; 25:1754–1760. [PubMed: 19451168]
61. Jurka J, et al. Repbase Update, a database of eukaryotic repetitive elements. *Cytogenet Genome Res*. 2005; 110:462–467. [PubMed: 16093699]
62. Bolger AM, Lohse M, Usadel B. Trimmomatic: a flexible trimmer for Illumina sequence data. *Bioinformatics*. 2014; 30:2114–2120. [PubMed: 24695404]
63. Bray NL, Pimentel H, Melsted P, Pachter L. Near-optimal probabilistic RNA-seq quantification. *Nat Biotechnol*. 2016; 34:525–527. [PubMed: 27043002]
64. McCarthy DJ, Campbell KR, Lun AT, Wills QF. Scater: pre-processing, quality control, normalization and visualization of single-cell RNA-seq data in R. *Bioinformatics*. 2017; 33:1179–1186. [PubMed: 28088763]

65. Robinson MD, McCarthy DJ, Smyth GK. edgeR: a Bioconductor package for differential expression analysis of digital gene expression data. *Bioinformatics*. 2010; 26:139–140. [PubMed: 19910308]
66. Haghverdi L, Buettner F, Theis FJ. Diffusion maps for high-dimensional single-cell analysis of differentiation data. *Bioinformatics*. 2015; 31:2989–2998. [PubMed: 26002886]
67. Liu X, et al. Distinct features of H3K4me3 and H3K27me3 chromatin domains in pre-implantation embryos. *Nature*. 2016; 537
68. Brin d'Amour J. An ultra-low-input native ChIP-seq protocol for genome-wide profiling of rare cell populations. *Nat Commun*. 2015; 6:6033. [PubMed: 25607992]
69. Neph S, et al. BEDOPS: high-performance genomic feature operations. *Bioinformatics*. 2012; 28:1919–1920. [PubMed: 22576172]
70. Zang C, et al. A clustering approach for identification of enriched domains from histone modification ChIP-Seq data. *Bioinformatics*. 2009; 25:1952–1958. [PubMed: 19505939]
71. Ramskold D, et al. Full-length mRNA-Seq from single-cell levels of RNA and individual circulating tumor cells. *Nat Biotechnol*. 2012; 30:777–782. [PubMed: 22820318]
72. Ponnaluri VKC, et al. NicE-seq: high resolution open chromatin profiling. *Genome Biol*. 2017; 18:122. [PubMed: 28655330]
73. Langmead B, Salzberg SL. Fast gapped-read alignment with Bowtie 2. *Nat Methods*. 2012; 9:357–359. [PubMed: 22388286]
74. Zhang Y, et al. Model-based analysis of ChIP-Seq (MACS). *Genome Biol*. 2008; 9
75. Ramirez F, et al. deepTools2: a next generation web server for deep-sequencing data analysis. *Nucleic Acids Res*. 2016; 44:W160–165. [PubMed: 27079975]
76. Quinlan AR, Hall IM. BEDTools: a flexible suite of utilities for comparing genomic features. *Bioinformatics*. 2010; 26:841–842. [PubMed: 20110278]

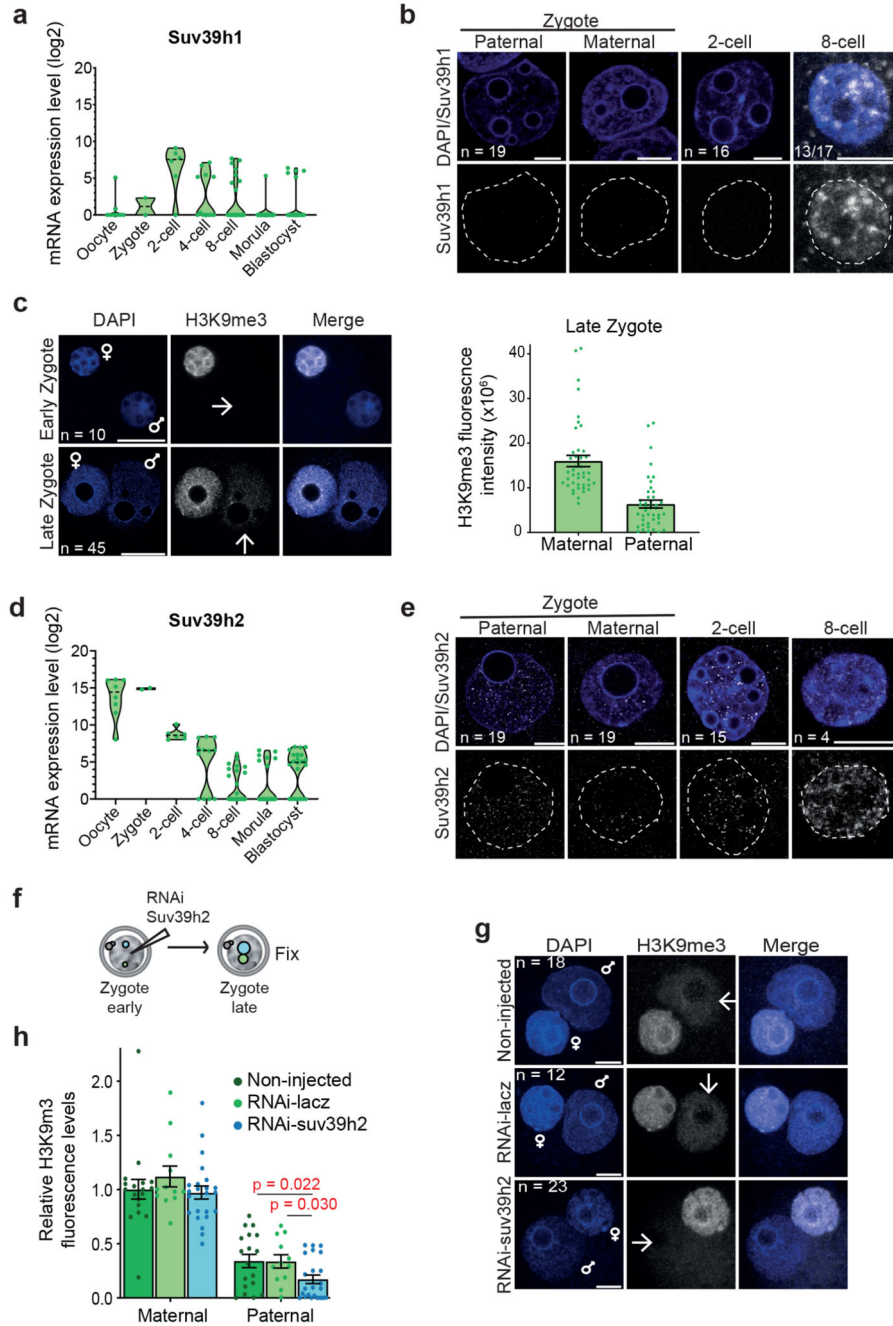


**Figure 1. De novo H3K9me3 occurs in the paternal pronucleus immediately after fertilization.**  
**a.** Violin plots showing absolute unnormalised *Suv39h1* single cell expression data by qRT-PCR as described before<sup>11</sup>. The dashed line represents the median value. For a and d the number of embryos analysed at each stage is indicated from 2 independent experiments.  
**b.** Immunostaining for Suv39h1 in the mouse late zygote, 2-cell and 8-cell stage. A representative single confocal section is shown for both pronuclei (PN3-4) from 19 zygotes across 4 independent experiments and a single nucleus of the 2-cell stage (16 embryos) and

8-cell stage (13 of 17 embryos positive) from 3 independent experiments. White dashed lines demarcate the nuclear membrane. Scale bar 10  $\mu\text{m}$ .

**c.** Representative single z-confocal sections projections for the indicated number of embryos stained with anti-H3K9me3 from 2 (early; 19h post-human chorionic gonadotropin injection (hCG)) or 5 (late; 27h post-hCG) independent experiments. Paternal (arrow) and maternal pronuclei are indicated. Scale bar 20  $\mu\text{m}$ . Right: quantification of total H3K9me3 signal in late zygotes. The plot depicts the mean  $\pm$  S.E.M (n = 45 zygotes collected from 5 independent experiments).

**d.** Violin plots showing absolute unnormalised *Suv39h2* single cell expression data by qRT-PCR as described before<sup>11</sup>. The dashed line represents the median value. **e.** A representative single confocal section is shown for embryos immunostained with anti-Suv39h2 from 1 (8-cell), 3 (2-cell) or 4 (late zygote) independent experiments. The total number of embryos analysed across the above-mentioned experiments are indicated. White dashed lines demarcate the nuclear membrane. Scale bar 10  $\mu\text{m}$ .

**f.** Experimental design for knockdown of Suv39h2 in zygotes.

**g.** Representative maximum intensity projections of zygotes treated as in f. Arrows point to the paternal pronuclei. Five independent experiments were performed for Suv39h2 knockdown and three for the control knockdown (RNAi-lacz). Scale bar 10  $\mu\text{m}$ .

**h.** Quantification of H3K9me3 fluorescence intensity in g. H3K9me3 fluorescence intensities were normalized to the mean maternal H3K9me3 signal in non-injected zygotes per experiment. Data is presented as mean  $\pm$  S.E.M (n = the total number of embryos analysed across experiments as indicated in g). The two-sided Mann-Whitney U-test was used for statistical analysis. Statistical source data are shown in Source data fig. 1.

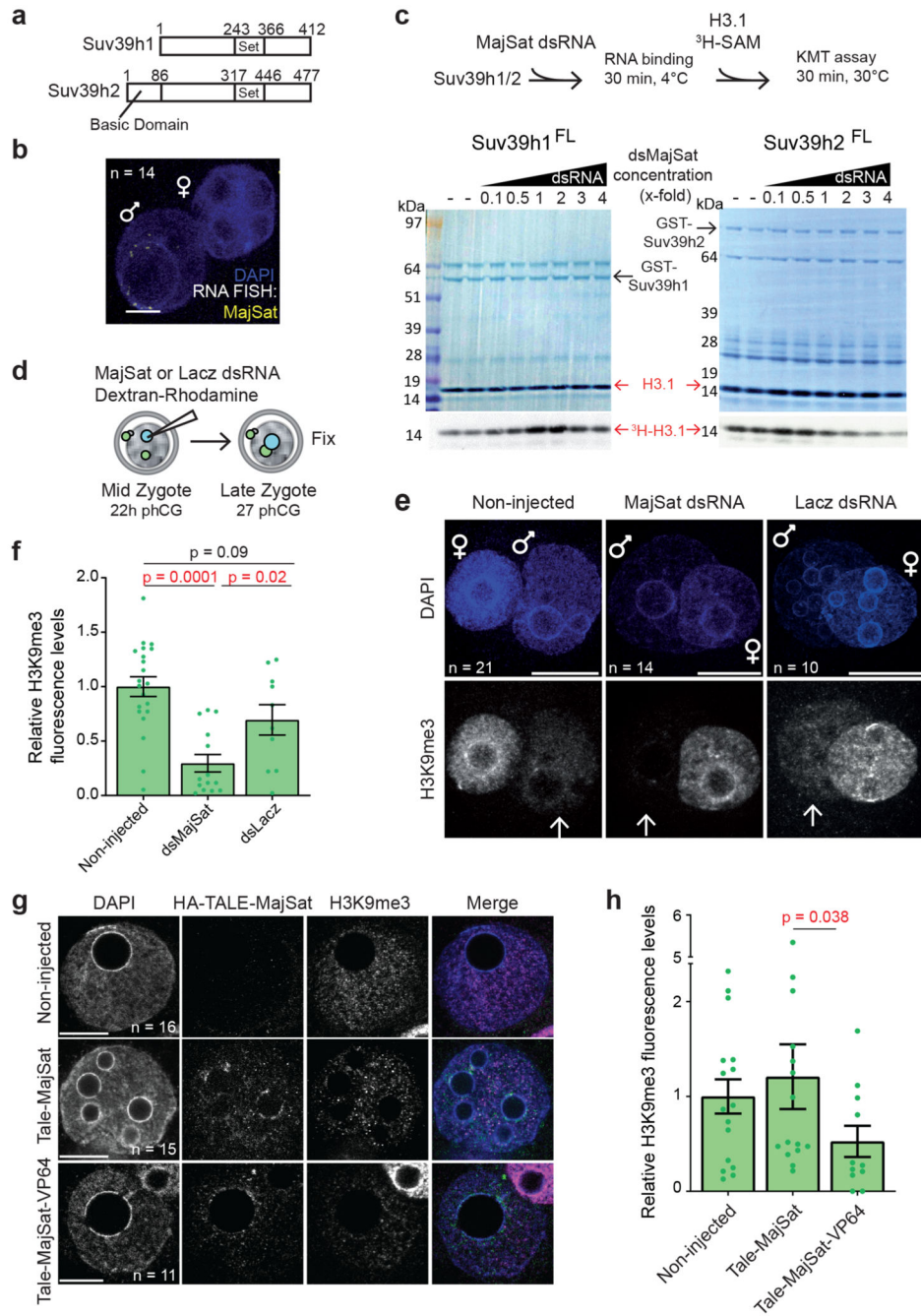


**Figure 2. Pericentromeric RNA modulation of the KMT activity of Suv39h2 attenuates H3K9me3 levels in the early preimplantation mouse embryo.**

**a.** Diagram depicting the alignment of *Mus musculus* Suv39h1 (NP\_035644.1) and Suv39h2 (NP\_073561.2) proteins. The sequences have a 58% identity and 71% similarity, excluding the N-terminal basic domain.

**b.** Representative full z-series confocal projection of RNA-FISH for Major Satellites in 14 zygotes across 3 independent experiments. Scale bar 10 μm.

- c.** In vitro KMT assays using full-length Suv39h1 or Suv39h2 after incubation with dsRNA from Major Satellites. Coomassie and autoradiography after KMT assay are shown. For Suv39h2 a downregulation of activity is observed in 4 out of 9 experiments (shown is a representative experiment of these 4) whereas no downregulation is observed for Suv39h1 across 7 experiments.
- d.** Experimental design: zygotes were collected 22 hours post hCG injection and the paternal pronucleus was injected with major satellite dsRNA or dsLacZ and dextran-rhodamine as injection control. Zygotes were cultured for 5 hours before fixation and immunostained with an anti-H3K9me3 antibody.
- e.** Representative full z-series confocal projections of embryos manipulated as described in d from the indicated number of embryos across 4 independent experiments (3 for RNAi-lacZ). Arrows point to the paternal pronuclei. Scale bar 10  $\mu$ m.
- f.** Quantification of mean fluorescence intensity for H3K9me3 in e. Confocal stacks were reconstructed in 3D using IMARIS and the pronuclei were segmented using the DAPI channel. The average levels of H3K9me3 staining in the paternal pronucleus were quantified after background subtraction and normalized to the non-injected group. Shown is the mean  $\pm$  S.E.M (n = the numbers indicated in e). The two-sided Mann-Whitney U-test was used for statistical analysis.
- g.** Zygotes microinjected with HA-TALE-VP64 mRNA targeting Major Satellites or control HA-TALE-MajSat without VP64 were fixed at 27h post-hCG (9 hours later) and immunostained for anti-HA and anti-H3K9me3. Shown are representative single sections of confocal stacks for the indicated number of embryos from 3 independent experiments. Scale bar 10  $\mu$ m.
- h.** Mean  $\pm$  S.E.M. of H3K9me3 levels in the paternal pronucleus across embryos in g (n = the numbers indicated in g). Statistical analysis was performed using the two-sided Mann-Whitney U test. Statistical source data and unprocessed blots are shown in Source data fig. 2.

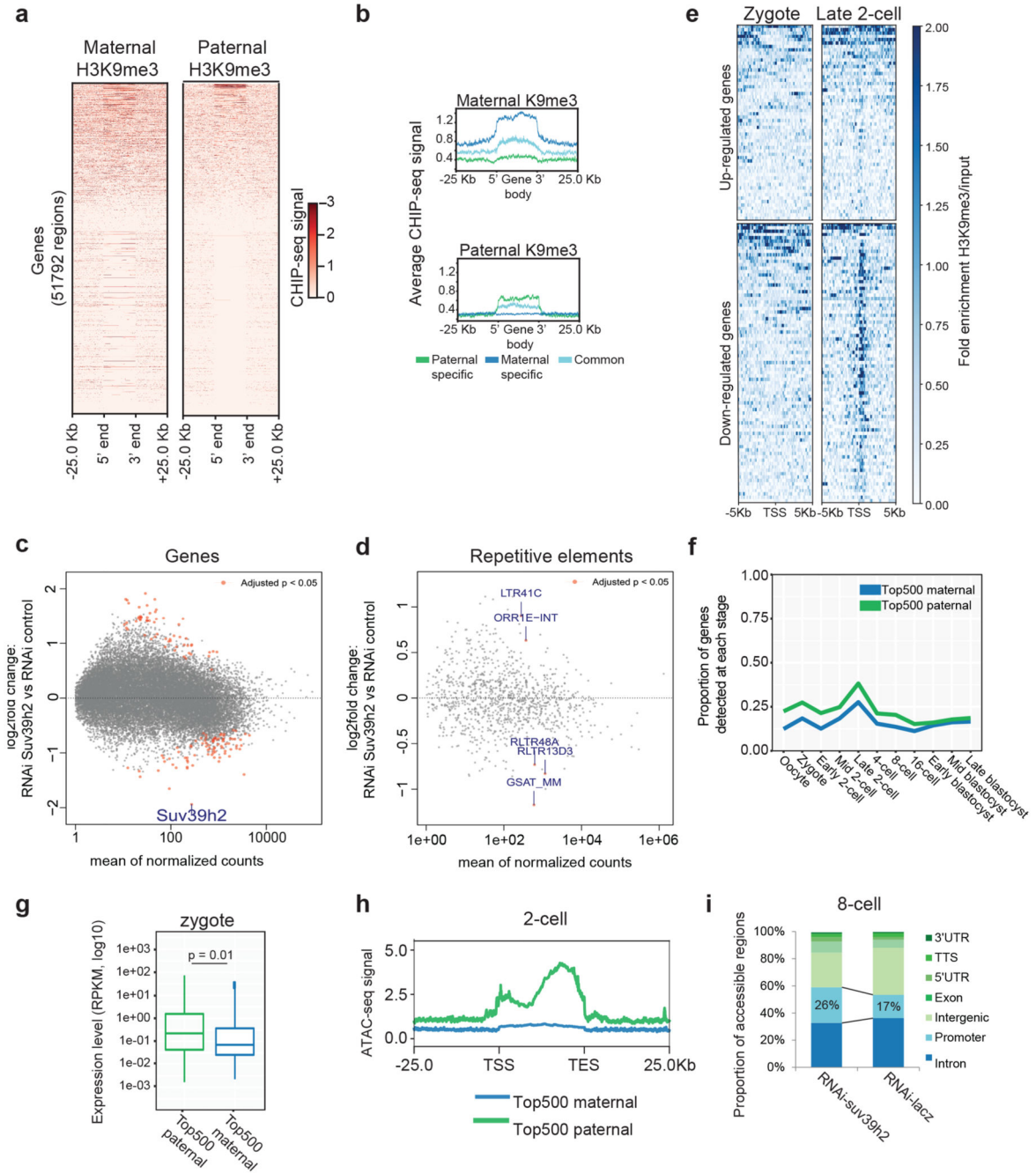


**Figure 3. H3K9me3 is compatible with gene expression during early preimplantation development.**

**a.** Heatmap of Zygotic H3K9me3 ChIP-seq signal over gene bodies, sorted by paternal pronucleus enrichment. Published H3K9me3 Chip-seq data<sup>12</sup> was reanalyzed for panels a, b, e, f and g.

**b.** Metagene plots showing the distribution of maternal or paternal H3K9me3 over gene bodies. Genes were classified according to whether they overlapped an H3K9me3 peak exclusively in the maternal allele, exclusively in the paternal allele or in both alleles.

- c-d.** RNA sequencing performed on 6 pools for RNAi-Suv39h2 and 5 pools for RNAi-LacZ injected embryos at the late 2-cell stage (46h post-hCG), collected from 3 independent experiments. Each pool consisted of 5 embryos. Differential expression analysis was performed using DESeq2. MA plot depicts log<sub>2</sub> fold change in expression levels for genes (c) and repetitive elements (d) on the y-axis, against the mean expression on the x-axis, with those with a significant change (p-adjusted <0.05) shown in red (listed in Table S3).
- e.** H3K9me3 ChIPseq signal at the TSS ( $\pm 5$  kbp) of differentially expressed genes after Suv39h2 knockdown versus knockdown control, in mid zygote and late 2-cell stage. Downregulated genes acquire clear H3K9me3 enrichment at the TSS by the 2-cell stage.
- f.** Proportion of top 500 maternal- or paternal-H3K9me3-marked genes expressed at each stage. Gene expression data for f and g were derived from ref.22.
- g.** Expression levels of top 500 maternal- or paternal-H3K9me3-marked genes in the zygote. The box plot depicts the median and interquartile range; whiskers span the range of the data, while extending no further than 1.5x the interquartile range. The two-sided students T-test was used to assess statistical significance.
- h.** Average ATAC-seq signal in the 2-cell stage over gene bodies of the top-500 Zygotic-H3K9me3-enriched genes in the maternal and paternal genomes. Data were derived from a published data-set<sup>23</sup>.
- i.** Proportion of genomic features enriched by NicE-seq in Suv39h2 knockdown 8-cell stage embryos compared to controls. The total number of peaks identified was similar between the two conditions (12,449 vs 11,922). Data shown represent results pooled from 10 8-cell stage embryos across 3 independent experiments.

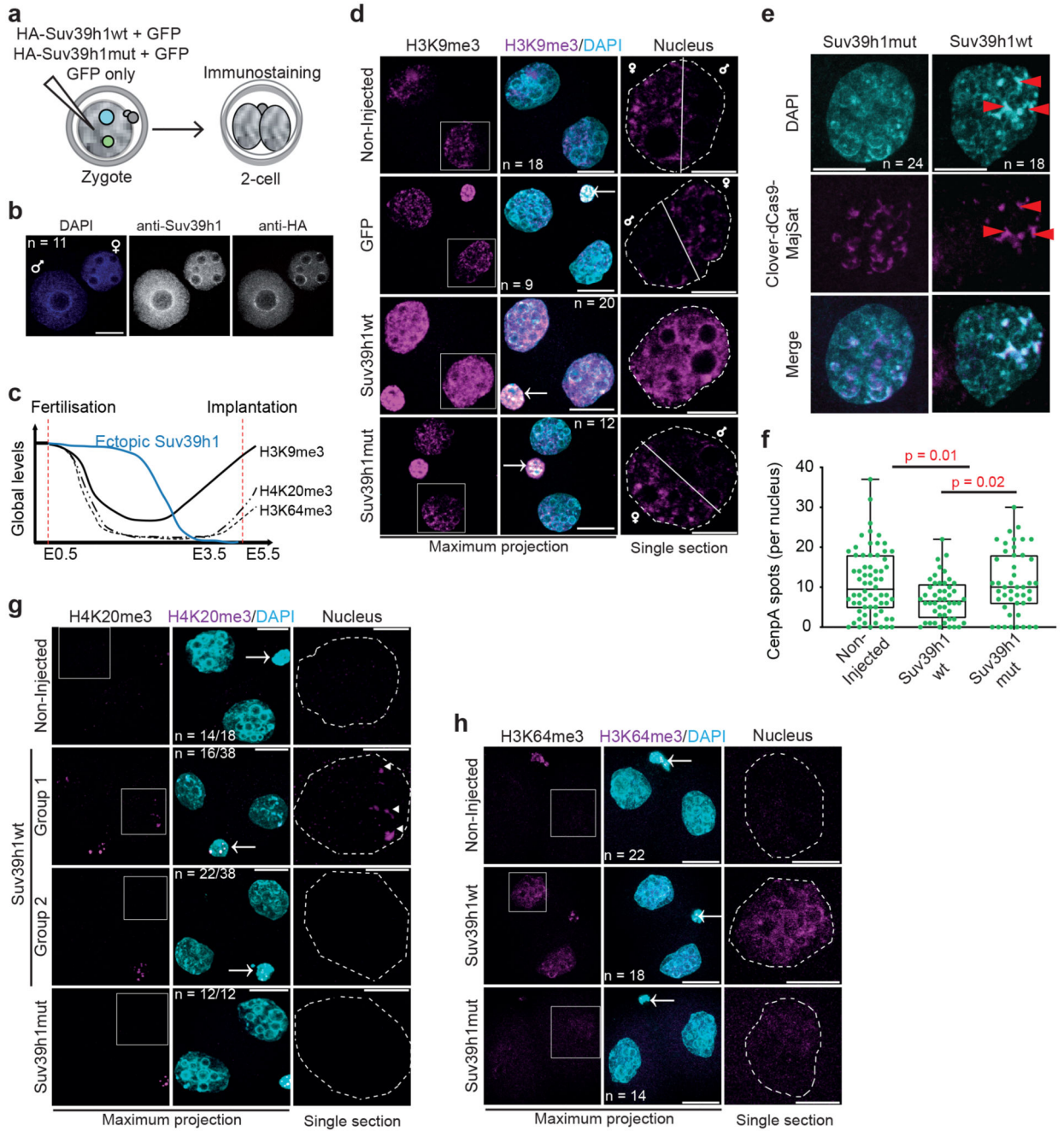


**Figure 4. Suv39h1 induces constitutive heterochromatin**

**a.** Diagram showing the experimental design.

**b.** A representative full z-series projection of 11 zygotes injected with HA-Suv39h1 mRNA, fixed and immunostained with anti-Suv39h1 and anti-HA 8 hours later from 3 independent experiments. Scale bar 10  $\mu$ m.

**c.** Summary of the dynamics of global levels of heterochromatic histone modifications in the preimplantation mouse embryo and the transient ectopic SUV39H1 expression. E, indicates embryonic day.

**d.** Representative full z-series confocal projections for embryos manipulated as indicated in a. The right-hand panel depicts a representative single confocal section of an individual nucleus indicated by the boxed region on the H3K9me3 panel. The white solid line highlights the segregation of the maternal and paternal genomes in the controls but not Suv39h1wt-injected embryos (see Supplementary Videos for 3D reconstructions). White dashed lines indicate the nuclear membrane. N = total number of embryos analysed across 6 independent experiments for Suv39h1wt and 2 for Suv39h1mut. Scale bar 20  $\mu\text{m}$  and 10  $\mu\text{m}$  for nuclear zooms. Where visible, the polar body is indicated by an arrow in the merge panel.

**e.** Zygotes microinjected with dCas9-mClover plus sgRNAs targeting Major Satellites and HA-Suv39h1wt or HA-Suv39h1mut mRNA (18 hphCG) were fixed at the 2-cell stage (42h phCG) and immunostained with an anti-GFP antibody. A representative full z-series projection of the indicated number of embryos from 5 independent experiments is shown. Red arrows indicate DAPI-intense, major satellite-positive clusters. Scale bar 10  $\mu\text{m}$ .

**f.** Mean number ( $\pm$  S.E.M.) of CenPA foci per nuclei was performed by blind counting for the number of embryos in e. Statistical analysis was performed using the two-sided Mann-Whitney U test.

**g.** As d. for H4K20me3. N = total number of embryos analysed across 3 independent experiments. The Suv39h1wt-injected group showed two patterns; either a strong increase around the nucleolar-like bodies (arrowheads) (group 1) or no H4K20me3 accumulation (group 2). The proportion of nuclei showing each pattern is indicated, determined through blind analysis.

**h.** As d. for H3K64me3. N = total number of embryos analysed across 5 independent experiments for Suv39h1wt and 4 for Suv39h1mut. Statistical source data are shown in Source data fig. 4.

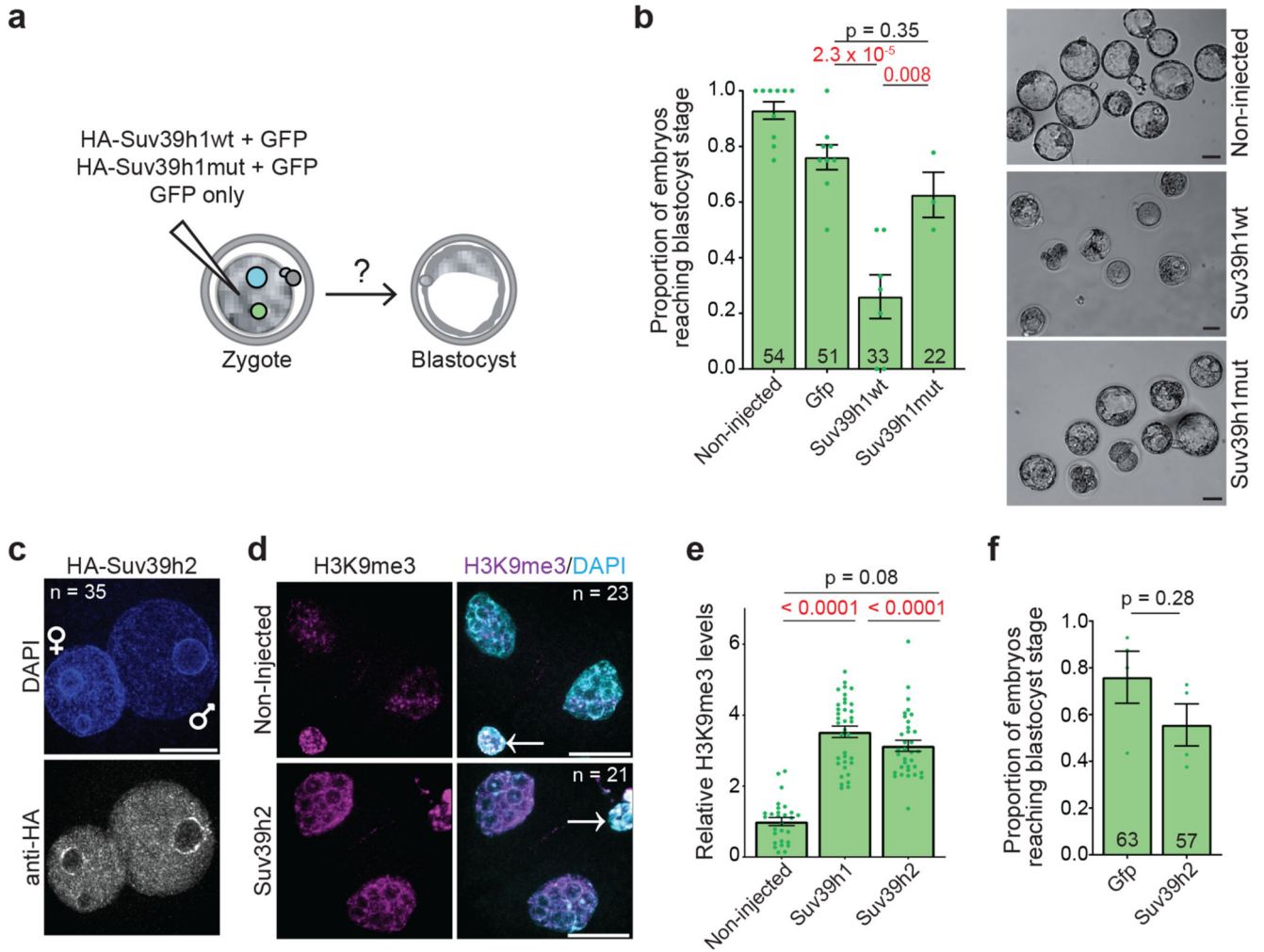


**Figure 5. Suv39h1 compromises development**

**a.** Diagram showing the experimental design.

**b.** The proportion of embryos that reached the blastocyst stage 72 hours after microinjection. Data show represent mean  $\pm$  S.E.M. (n = the total number of embryos analysed as indicated on the graph across 6 independent experiments for Suv39h1wt and 3 independent experiments for Suv39h1mut). Statistical analysis was performed using the N-1 Chi-squared test for comparing independent proportions. On the right are shown representative brightfield images of embryos injected at the zygote stage with Suv39h1 wt or mut mRNA and cultured to the blastocyst stage (72h after microinjection). Scale bar 50  $\mu$ m.

**c.** A representative full z-series confocal projection of 35 zygotes injected with HA-Suv39h2 mRNA, fixed and immunostained with anti-HA 8 hours later from 3 independent experiments. Scale bar 10  $\mu$ m.

**d.** Zygotes were microinjected with HA-Suv39h2 mRNA and fixed at the 2-cell stage, 24 hours after microinjection and immunostained with an anti-H3K9me3 antibody. A representative full z-series confocal projection is shown from 3 independent experiments (n refers to the total number of embryos analysed). Scale bar 20  $\mu$ m. Where visible, the polar body is indicated by an arrow in the merge panel.

**e.** Mean levels of H3K9me3 in the 2-cell stage embryo after Suv39h1wt or Suv39h2 mRNA injection for the embryos represented in d. Error bars represent S.E.M. (n = the total number of embryos analysed as indicated in d across 3 independent experiments). Statistical analysis was performed using the unpaired students T test

**f.** The proportion of embryos that reached the blastocyst stage 72 hours after microinjection. Data show represent mean  $\pm$  S.E.M. (n = the total number of embryos analysed as indicated on the graph across 4 independent experiments). Statistical analysis was performed using the N-1 Chi-squared test. Statistical source data are shown in Source data fig. 5.

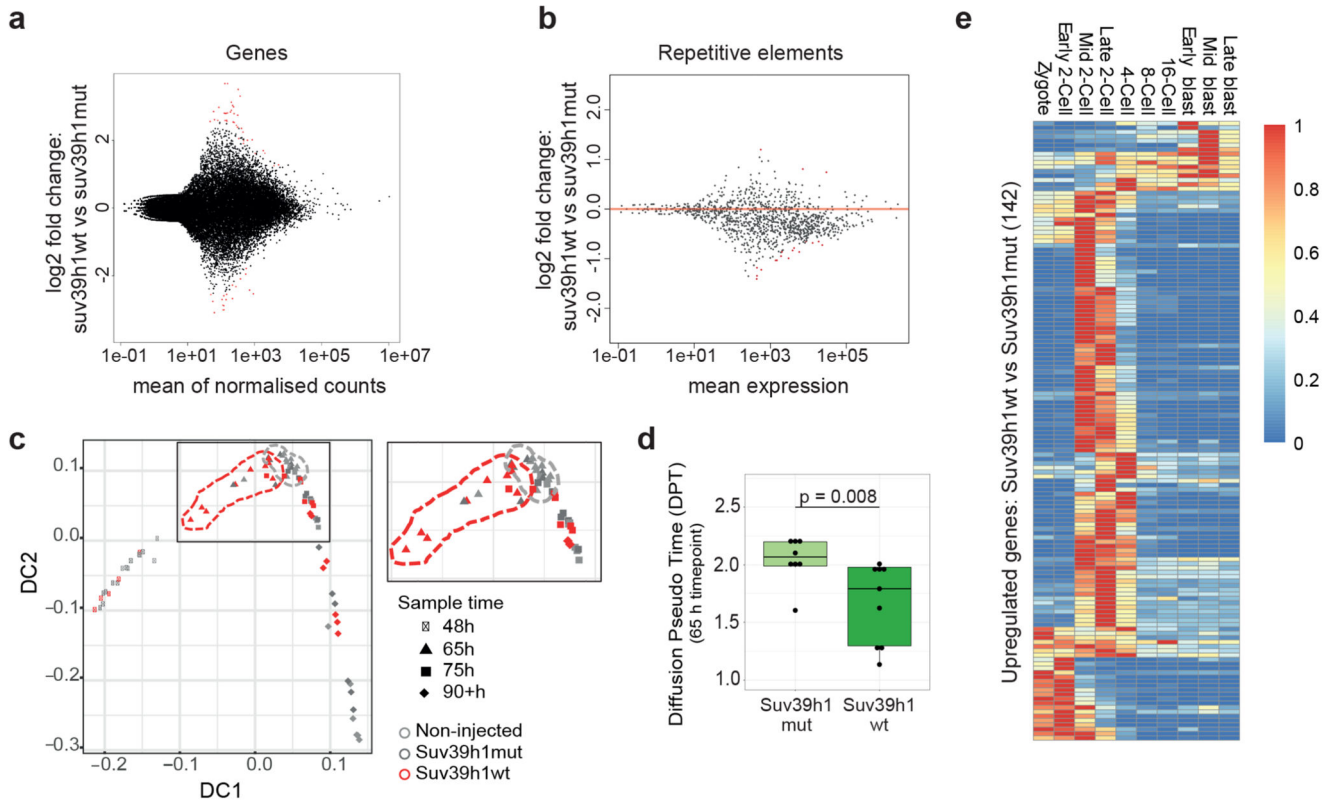


**Figure 6. Suv39h1 does not prevent zygotic genome activation**

**a-b.** RNA sequencing was performed on embryos expressing *Suv39h1*wt and *Suv39h1*mut at the late 2-cell stage (46h post-hCG), in two pools of 20 embryos per condition; each pool was collected from 3 independent experiments. Differential expression analysis was performed using DESeq2. The MA plot depicts log<sub>2</sub> fold change in gene a. or repetitive element b. expression levels, against the mean expression, with those with a significant change ( $p$ -adjusted <0.05) shown in red (listed in Tables S7–8).

**c.** Diffusion map of the single embryo RNA-Seq RPKM counts. The dashed areas indicate the relative positions of the *Suv39h1*wt embryos at 65h (4-cell stage) in red and the combined controls at 65h in grey. Embryos at all time points were collected from 4 independent experiments including the 3 sample groups.

**d.** Diffusion pseudotime distribution values of embryos expressing *Suv39h1*wt ( $n = 9$ ) and *Suv39h1*mut ( $n = 8$ ) at the 65h timepoint.  $N$  = the indicated number of embryos from 4 independent experiments. The box plots represent the mean with interquartile range. Statistical analysis was performed using the two-sided Mann-Whitney U test.

**e.** Heatmap depicting the endogenous expression patterns of the up-regulated genes between embryos expressing *Suv39h1*wt vs *Suv39h1*mut at the 65 hours timepoint (4-cell stage). Scaled RPKM counts are shown. RNAseq datasets are from ref. 22.

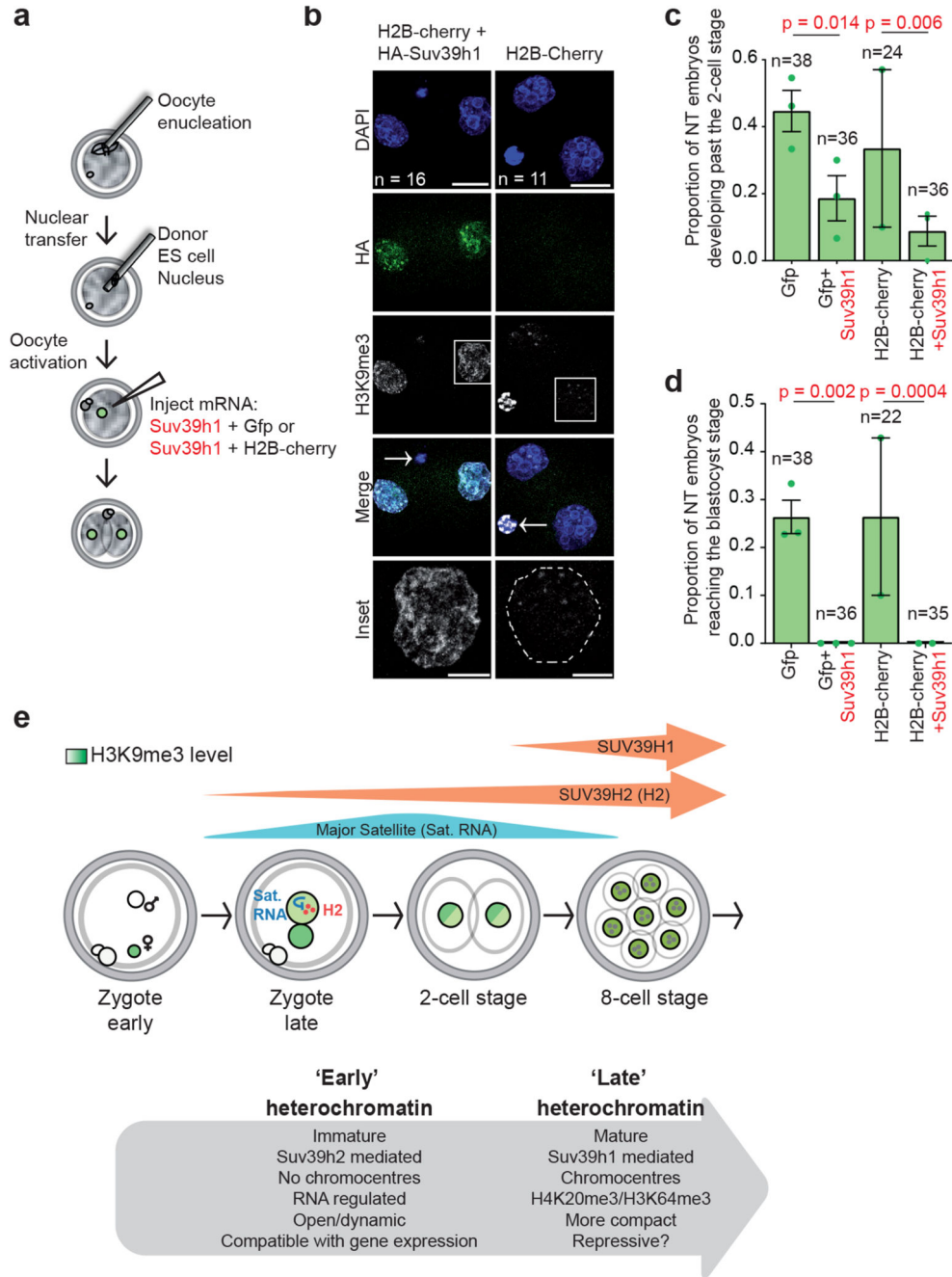


**Figure 7. Suv39h1 inhibits epigenetic reprogramming**

**a.** Experimental design for nuclear transfer and microinjection. Nuclear transfer was performed using an ES cell nucleus as donor. Four hours after activation, oocytes were microinjected with mRNA for Suv39h1 wt and GFP or GFP alone or using an alternative control Suv39h1 wt and H2B-cherry or H2B-cherry alone and cultured until the blastocyst stage.

**b.** Representative full confocal z-series projections of embryos manipulated as described in **a.** fixed at the 2-cell stage and immunostained with anti-HA and anti-H3K9me3 antibodies.

N = total number of embryos analysed from 4 independent experiments. The inset shows a higher magnification of the H3K9me3 staining in the boxed single nucleus. White dashed lines indicate the nuclear membrane in the control inset panel and the polar body is indicated by an arrow in the merge panel. Scale bar 20  $\mu\text{m}$  (10  $\mu\text{m}$  for insets).

**c.** The proportion of embryos developing beyond the 2-cell stage. Data shown represent mean  $\pm$  S.E.M. (n = the total number of embryos analysed as indicated on the graph across 3 independent experiments, except for H2B-cherry alone where 2 independent experiments were performed). Statistical analysis was performed using the N-1 chi-square test for comparing independent proportions.

**d.** The proportion of nuclear transfer embryos developing to the blastocyst stage. Data shown represent mean  $\pm$  S.E.M (n = the total number of embryos analysed is indicated on the graph across 3 independent experiments, except for H2B-cherry alone where 2 independent experiments were performed). Statistical analysis was performed using the N-Chi-squared test. Statistical source data are shown in Source data fig. 7.

**e.** Model summarizing our findings.